SECTION I

NUCLEAR STRUCTURE

NUCLEAR REACTIONS

Probing the Nuclear Stratosphere with Sub-Coulomb Heavy Ion Elastic Scattering

W.G. Lynch, M.B. Tsang, Dan Fox, J.G. Cramer*, R. Loveman*, S. Gil* and D. Leach*

Recently evidence has accumulated indicating the importance of dynamical deformations in sub-barrier heavy ion fusion reactions.[1] Similar deformations have for some time been considered an important aspect of deeply inelastic reactions. We are examining sub-Coulomb heavy ion elastic scattering to determine whether such deformations are important to the elastic channel.

Preliminary evidence from $^{12}C + ^{208}Pb$ data indicates that the real optical potential dominates the imaginary potential in these heavy ion systems[2] therefore it should be possible to search for dynamical deformations provided sufficiently good real optical potentials are available to describe the nuclear interaction in the sudden approximation. In the absence of dynamical deformations the elastic scattering should be well described by doubly folded real optical potentials[3] since the low density approximation is well satisfied. There are indications from fusion data, however, that the $^{16}O + ^{208}Pb$ system appears to be considerably deformed[1] at about 13 fm and if these deformations persists at larger radii they should be easily observed in elastic scattering.

We have measured elastic scattering with fixed angle excitation functions with the projectiles ^{12}C, ^{16}O, and ^{18}O on the target nucleus ^{208}Pb using the University of Washington tandem Van de Graff. The angles measured were $\pm 30^{o}$, $\pm 145^{o}$, $\pm 150^{o}$, $\pm 160^{o}$, and $\pm 170^{o}$. The use of symmetrically placed detectors on both sides of the beam and a 1 mm strip ^{208}Pb target enabled elimination of systematic errors due to variations in beam phase space. Care was taken to limit other sources of systamatic error so that the final fractional systematic error is less than 5×10^{-4}.

Preliminary data for ^{16}O and ^{18}O projectiles are presented in Fig. 1 and 2 respectively. The errors quoted are purely statistical and systematic corrections of a few tenths of percent magnitude have yet to be applied. We plot Δ_{nuc} (the deviation from Rutherford scattering caused by the nuclear interaction) versus R_{tp} the classical turning point where

$$R_{tp} = Z_1 Z_2 e^2 \, (1 + \csc(\theta_{cm}/2))/(2E_{cm}).$$

At present, the data have not been corrected for the small effects caused by atomic screening, vacuum polarization, nuclear polarization, and relativity,[4] therefore we approximate Δ_{nuc} by

$$\Delta_{nuc} = 1 - Y(\theta, E)\, Y(30^{o}, E_c)/(Y(30^{o}, E)\, Y(\theta, E_o)) \approx 1 - sig(\theta, E)/sigR(\theta, E)$$

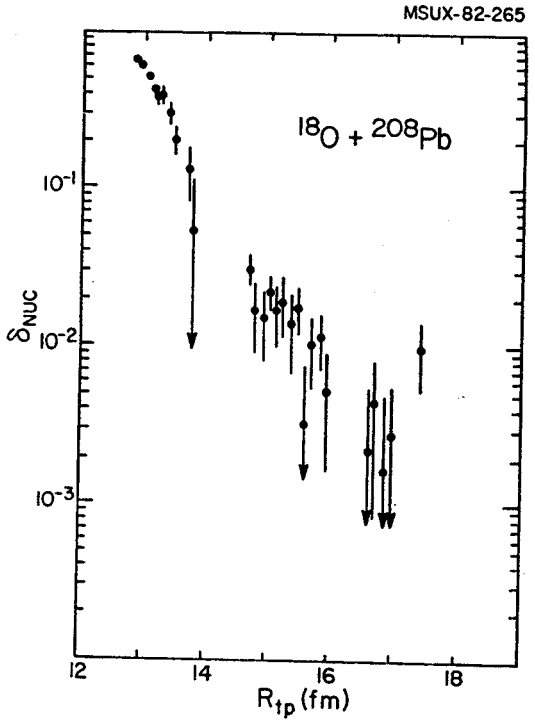

Fig. 1.

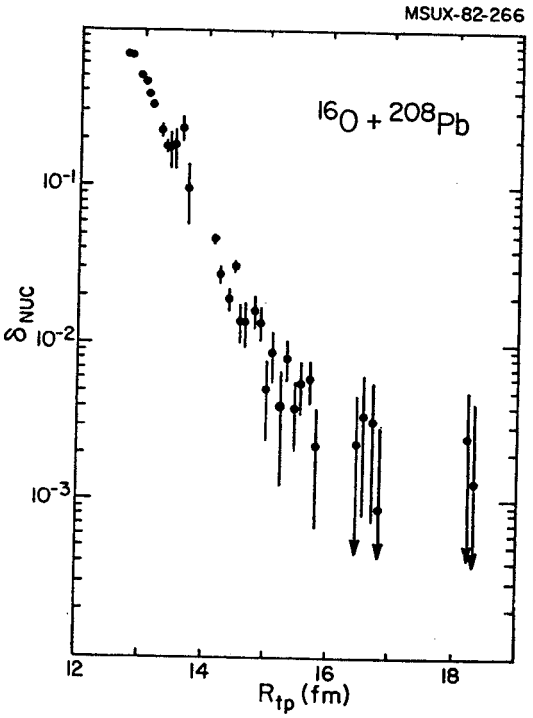

Fig. 2

where $Y(\theta,E)$ is the measured yield and ($sig(\theta,E)$, $sigR(\theta,E)$) are the (optical model cross section, Rutherford cross section) respectively at scattering angle θ and bombarding energy E. E_o is some suitably chosen bombarding energy well below the Coulomb barrier where nuclear interactions are vanishingly small.

The available folding model prescriptions only specify the real potential.[1] One can use our measured direct reaction data to obtain the imaginary potential since fusion cross section is very small at these energies. We are currently summing the inelastic and transfer peaks to obtain the reaction cross section. Preliminary results for the ^{16}O data indicate that the optical model absorption accounts for less than 30% of the observed deviation. This is in qualitive agreement with previous results with ^{12}C projectiles.[2]

Quantitative comparison of the data with folding model calculations will have to wait until final analysis of the data. Nevertheless comparison of the preliminary data shows the ^{18}O potential to be considerably more diffuse than the ^{16}O or ^{12}C potential whereas previous studies have indicated that the ^{12}C potential is already quite diffuse (1 fm) at sub-Coulomb energies.

---

* Nuclear Physics Laboratory, University of Washington, Seattle, WA 98195.

1. L.C. Vaz et al., Phys. Rep. 69, (1981) 373.
2. W.G. Lynch, Ph.D. Thesis, University of Washington, Seattle, WA.
3. G.R. Satchler and W.G. Love, Phys. Rep. C55, (1979) 183.
4. W.G. Lynch et al., Phys. Rev. Lett. 48, (1982) 979.

A Measurement of the Electric Polarizability of the Deuteron

W.G. Lynch, N.L. Rodning*, L.D. Knutson*, G. Orr*, and M.B. Tsang

Since the early work of Oppenheimer and Phillips[1], calculations have predicted that when the deuteron is in close proximity to a highly charged nucleus such as ^{208}Pb, the deuteron should be strongly polarized by the Coulomb field of that nucleus. Our interest in the electric polarizability of the deuteron stems from the fact that although it is a fundamental property of the n-p system, it has not been measured.

Calculations of the electric polarizability of the deuteron have been reported by a number of authors[2-7] and a variety of calculational methods have been used. To a very good approximation the induced electric dipole moment is given by $\bar{P} = \bar{E}_c$ where E_c is the Coulomb field of the heavy nucleus and α is the polarizability. While values of α ranging from .21 to .64 fm^3 have been reported, it appears that a reasonable estimate is about .60 fm^3.

We have measured the electric polarizability of the deuteron by measuring elastically scattered deuterons from the target nucleus ^{208}Pb using the University of Wisconsin tandem Van de Graff. The experiment was performed at sub-Coulomb bombarding energies ranging from 3-7 MeV and at scattering angles of $\theta_{lab} = \pm 60^\circ$, $\pm 140^\circ$, $\pm 150^\circ$, $\pm 160^\circ$. Data at $\pm\theta$ about the beam axis were combined to eliminate odd order effects due to beam motion on the target. At some energies and angles, (d,p) and (d,α) reactions from C, O and N target contaminants had to be subtracted from the d+^{208}Pb elastic peaks. An energy spectrum showing these contaminants is shown in Fig. 1. To enable this subtraction, these (d,α) and (d,p) reactions were measured using a carbon target which contained a significant oxygen contamination and also a melamine target to obtain the nitrogen cross sections. Except at 7 MeV where the contaminant correction was about 10%, the contaminant subtraction from the d+^{208}Pb elastic peak was the order of a few tenths of a percent.

We plot the experimental ratio

$$R(E) = \frac{\sigma(3\ \text{MeV}, 60^\circ)/\sigma(3\ \text{MeV}, \theta)}{\sigma(E, 60^\circ)/\sigma(E, \theta)}$$

where $\theta = 140^\circ$, 150°, 160° in Fig. 2. Since the angular dependence of Rutherford scattering is energy independent, this ratio is 1 for purely Rutherford scattering. Also indicated on the Fig. are calculations for the various background effects such as screening, vacuum polarization, relativity and nuclear interactions. The first three effects have been previously measured and are well enough understood[8]. The nuclear interaction effects were calculated using an

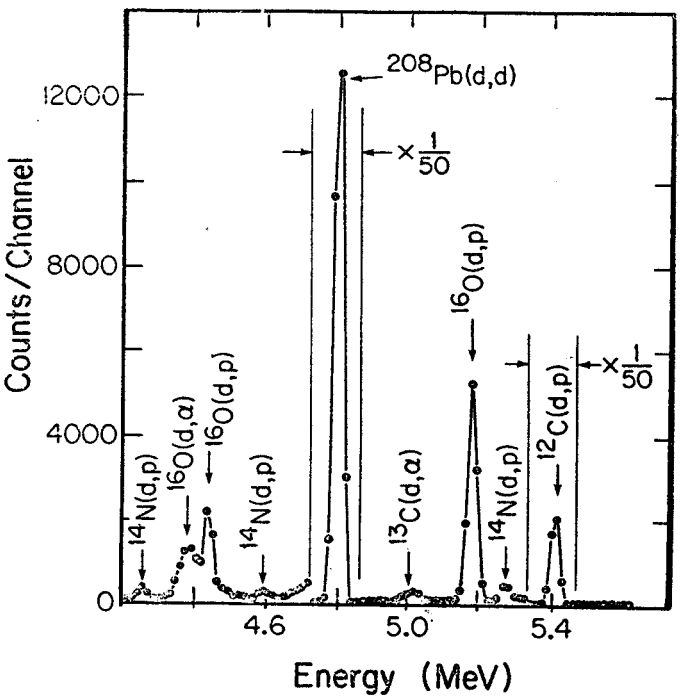

Fig. 1. A typical pulse height spectrum obtained with E_d=5 MeV and θ=160°.

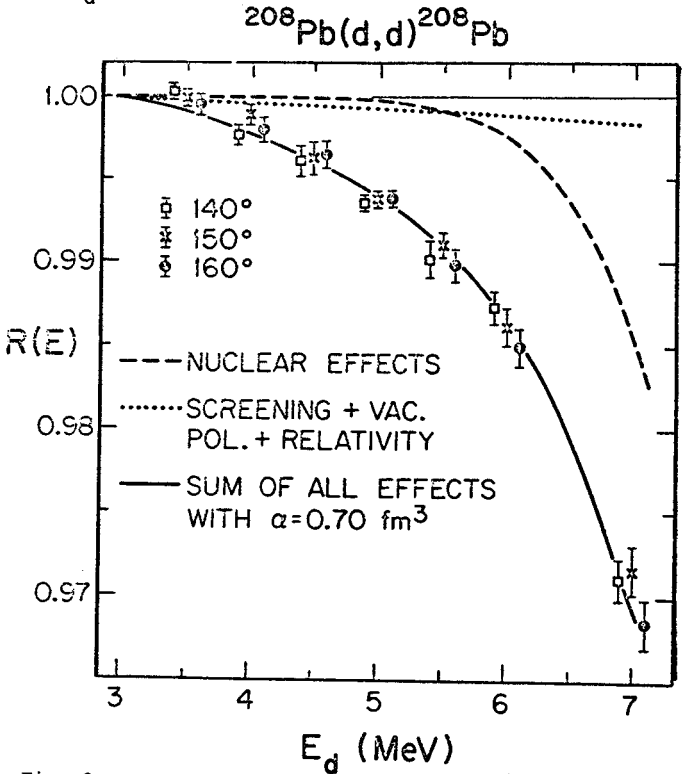

Fig. 2. Measurements of R(E) for $\theta = 140^\circ$, 150° and 160°. The dotted curve shows the sum of the contributions to R from atomic screening, relativistic corrections, and vacuum polarization, while the dashed curve is an estimate of the effects of nuclear processes. The solid curve includes these effects as well as the calculated effect of the electric polarizability of the deuteron, with α=0.70 fm^3. The curves are for $\theta = 150^\circ$.

optical potential which was constrained to reproduce the total reaction cross section consisting primarily of (d,p) reactions. By introducing this constraint and varying the optical model parameters within reasonable limits, it was observed that the nuclear interaction effects were well predicted by the reaction cross-section input alone.

Taking these corrections into consideration and introducing a theoretical error to the nuclear interaction correction equal to the magnitude of the nuclear correction we obtain α by fitting the data for $E_{lab} \leq 5.5$ MeV. The value for

$$\alpha = .70 \pm .05 \text{ fm}^3$$

was used to obtain the solid curve in Fig. 2 which corresponds to a predicted deviation from Rutherford scattering with the previous discussed effects taken into consideration. We note that the solid curve accurately reproduces the measurement at 6.0 and 7.0 MeV although no attempt was made to fit this data. We take this as further evidence that our calculation of the nuclear effects is valid and our determination of α is correct.

Our measured value for α is in fair agreement although somewhat larger than theoretical predictions in the literature. Several calculations have given predictions of α as large as .63 or .64 fm^3. It may not be clear what constraints our measurement of α places on the deuteron wave functions until calculations are performed using modern n-p interactions and including mesonic degrees of freedom in the deuteron wave function. It is our hope that such calculations of α will be performed for the deuteron and also other light nuclei. Should such calculations provide motivation for further experiments, it is our belief that with sufficient care one could make significantly more accurate measurements of α.

---

* Physics Department, University of Wisconsin, Madison.

1. J.R. Oppenheimer and M. Phillips, Phys. Rev. 48, 500 (1935).
2. C.F. Clement, Phys. Rev. 128, 2724 (1962).
3. N.F. Ramsey, B.J. Malenka and V.E. Kruse, Phys. Rev. 91, 1162 (1953).
4. J. Sawicki, Acta Phys. Polon. 13, 225 (1954).
5. B.W. Downs, Phys. Rev. 98, 194 (1955).
6. J.E. Kammeraad, private communication.
7. J.S. Levinder, Phys. Rev. 107, 554 (1957).
8. W.G. Lynch, M.B. Tsang, H.C. Bhang, J.G. Cramer and R.J. Puigh, Phys. Rev. Lett. 48, 979 (1982).

Mechanisms of the $^{6}Li(^{6}Li,2\alpha)\alpha$, $^{6}Li(^{6}Li,2\alpha)2d$, and $^{6}Li(^{6}Li,2d)2\alpha$ reactions at 97.5 MeV

K. Blum**, A. Galonsky, P. Schwandt*, D.K. Scott, P.P. Singh*, and R.E. Warner**

The $^{6}Li(^{6}Li,2\alpha)\alpha$ reaction may proceed by either direct capture of a deuteron by one ^{6}Li, with the remaining α-particle acting as a spectator, or sequential decay of an intermediate excited ^{8}Be level. The separation in the coincidence energy spectra of groups from these two processes increases as the bombarding energy rises.

Studies[1] of this reaction at 2 to 13 MeV were said to show the dominance of the spectator process; however, because of kinematical ambiguities, much of the yield could instead have resulted[2] from sequential decay of the 2.94 and 11.4 MeV ^{8}Be levels. At 36 to 46 MeV, the spectator process yield was never more than one-third of that due to sequential decay[2]; even with the improved separation at this energy, extraction of the spectator peak was difficult.

We have now made measurements at 97.5 MeV at the Indiana University Cyclotron Facility. Coincidence α-α spectra were obtained with two 2-counter telescopes coplaner with, and at equal angles on opposite sides of, the beam. Optimum conditions for the spectator process are at $\theta_1 = \theta_2 = 38^{\circ}$, where the undetected α-particle may be left at rest in the laboratory. The spectrum, shown in Fig. 1, is well fitted by spectator model predictions[2] which assume that a harmonic oscillator potential binds the α- and d- clusters into an s- state. Sequential decay from the levels near 20 MeV is well separated from the spectator peak, and that of lower-lying levels is still further removed. The spectator peak cross section, 4.5 mb/sr^2, is three times the target value observed near 40 MeV.

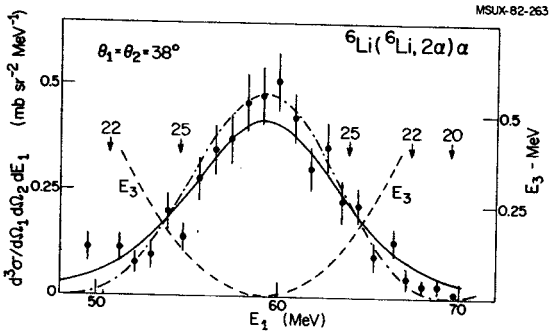

Fig. 1.

The cross section falls dramatically, as predicted by the spectator model, for detector angles $\theta_1 = \theta_2 = 42^{\circ}$ and 44°; at these geometries, the minimum spectator energies are about 0.5 and 1 MeV, respectively. In Table I observed cross sections (integrated from E_α=48 to 71 MeV) are compared with spectator model predictions

Table I. Predicted and measured cross sections (mb/sr^2) for $^{6}Li(^{6}Li,2\alpha)$ at 97.5 MeV.

Type	38.0°	42.0°	43.7°	46.4°
Harmonic Oscillator	4.45	0.32	0.52	0.23
Exterior square well	4.45	0.10	0.03	0.005
Tang-Wildermuth	4.45	1.28	0.25	0.003
Hulthén	4.45	0.89	0.04	0.03
Measured	4.45	0.36	0.18	0.41
$E_{3,min}$(MeV)	.001	0.49	1.08	2.63

utilizing four cluster wave functions used[3] for interpreting $^{6}Li(^{6}Li,\alpha\alpha)dd$ data. All predictions are normalized to the 38° yield. Sequential decay contributions increase with increasing angle, and so the spectator cross sections would drop even more sharply with angle if these contributions could be removed.

The 42° and 44° data sample the cluster momentum wave function $\Phi(p)$ at large p, and the predictions are sensitive to the interaction. Thus, the Tang - Wildermuth and Hulthén wave functions significantly over - predict the yield. The harmonic oscillator or square well predictions may be best, depending upon the amount of sequential decay contamination. An experiment at E_α = 150 MeV is being planned, which will yield data free of sequential decay for spectator particle energies up to 5 MeV. This will sensitively test the cluster wave function $\Phi(p)$ for large p, and may permit a determination of the d-state probability[4] in the ^{6}Li ground state.

The $^{6}Li(^{6}Li,2\alpha)2d$ and $^{6}Li(^{6}Li,2d)2\alpha$ reactions were studied to search for double spectator pole (DSP) events. In such an event two nuclei, each containing two clusters, collide with one cluster from each nucleus retaining its initial momentum. Weak evidence[5] for DSP behavior in the $^{3}He(^{3}He,dd)pp$ reaction was reported, and $^{2}H(^{2}H,pp)nn$ data were interpreted[6] by a DSP model but later shown[7] to be better fitted by a double - final - state-interaction model. More recently anomalously sharp peaks were observed[3] in both α-α and d-d coincidence spectra from ^{6}Li + ^{6}Li double breakup at E_o ~ 40 MeV, with their centers at those energies where the DSP is expected. Straightforward improvements[8] of the PWBA - DSP model--by adding symmetry under boson exchange, Coulomb cluster wave functions, deuteron structure, and a finite-range participant interaction potential--failed to change the predicted widths of

these peaks, which typically were five times as great as those observed.

Fig. 2 shows our α-α coincidence spectra from the $^{6}Li(^{6}Li,2\alpha)2d$ reaction 97.5 MeV. The spectra are for $E_{\alpha 1} = E_{\alpha 2}$, i.e. from the total available phase space, a cut is taken along the 45° line in the $E_{\alpha 1} = E_{\alpha 2}$ plane. The detector angles are uncertain by about 1°, as was found while performing energy calibration with the $^{2}H(^{6}Li,2\alpha)$ reaction. The DSP-model predictions have been shifted by amounts up to 2 MeV, to align them with the observed peaks. Such shifts are commensurate with the detector angle uncertainty.

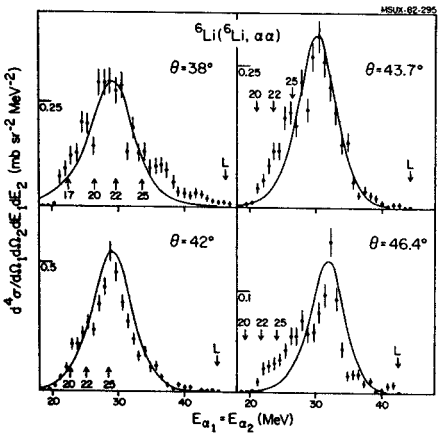

Fig. 2.

At this bombarding energy, the widths and shapes of the observed peaks are consistent with the predictions of the DSP model. Moreover, these peaks contain virtually all the yield between the detector threshold energy (~ 20 MeV) and the four - body kinematic limit (~ 45 MeV). Their strengths are comparable to those observed[3] at Chalk River; their widths are about 10 times and their amplitudes about 0.1 times, as great as in the 40 MeV data.

Cross sections for d-d quasi-elastic scattering (QFS) were found to be much smaller than those for α-α QFS, and there was less evidence for peaks having the DSP shape. This probably reflects a dominance of d+d breakup over elastic scattering at these bombarding energies.

---

* Indiana University Cyclotron Facility
** Oberlin College

1. L.L. Gadeken and E. Norbeck, Phys. Rev. Lett. 27 952 (1971); Phys. Rev. C 6 1172 (1972).
2. R.E. Warner, W.T. Conner, G.C. Ball, W.G. Davies, and A.J. Ferguson, Nucl. Phys. A341, 483 (1980).
3. R.E. Warner, G.C. Ball, W.G. Davies, and J.S. Forster, Nucl. Phys. A365, 142 (1982).
4. R. Hagelberg, E.L. Haase, and Y. Sakamoto, Nucl. Phys. A207, 366 (1973).
5. R.G. Allas, L.G. Beach, R.O. Bondelid, L.T. Myers, E.L. Peterson, J.M. Lambert, P.A. Treado, and I. Slaus, Nucl. Phys. A304, 461 (1978).
6. B.T. Leeman, H.G. Pugh, N.S. Chant, and C.C. Chang, Phys. Rev. C 17, 410 (1978).
7. R.E. Warner, Phys. Rev. C 24, 2759 (1978).
8. R.E. Warner, Nucl. Phys. A379, 191 (1982).

Fusion of ^{16}O with ^{12}C

J. Kasagi, A. Galonsky, F. Haas, B. Remington,
P. Deyoung*, R. Freeman*, J. Kolata*, R. Racca*,
L. Satkowiak*, M. Xapsos*, and F. Prosser**

In the reaction $^{16}O + ^{12}C$, the total fusion cross section, σ_f, has been shown to display two main features. First, at energies above the coulomb barrier, σ_f initially increases with increasing incident energy, and then, beyond $E_{c.m.} \cong 21$ MeV, it levels off to an almost constant value.[1] It is now suspected that this leveling off of σ_f, i.e., this "fusion-limiting mechanism," depends upon the properties of the compound system.[2] Secondly, structure has been seen in σ_f in the energy region 30 MeV $\leq E_{lab}(^{16}O) \leq 63$ MeV, but results obtained from charged particle detection are not entirely consistent with those obtained by detection of the gamma rays.[1,3]

Therefore, to further explore these features and questions, we conducted the following experiment on the tandem Van de Graaff accelerator at Notre Dame. We sought to determine the entry points of the different residual nuclei from the reaction $^{16}O + ^{12}C$ at seven incident (lab) energies varying from 43.2 MeV to 60.7 MeV. To this end we attempted to measure the average gamma ray multiplicity and also the average gamma ray multiplicity and also the average energy per gamma ray for each residual nucleus, thus allowing us to locate its average entry point. As a cross check, we measured the neutron energy spectra for each energy, and we are measuring the charged particle energy spectra.

The multiplicity measurement was performed as follows: A 107 cm^3 Ge(Li) detector was placed at 55° to the beam direction and six 10 cm x 10 cm NaI detectors were arranged at various angles about a lead-backed ^{12}C target, with two of the NAI detectors being out of the plane defined by the beam and the Ge(Li) detector. A copper disk approximately 3.2 mm thick was placed in front of each NaI detector to "flatten" its energy response. The data were digitized, stored on magnetic tape, and later sorted according to their k-fold coincidence, where k=# of NaI detectors in coincidence with the Ge(Li).

The gamma ray multiplicity, M, was calculated from

$$M = \frac{N_C}{N_S \varepsilon / 4\pi},$$

where

$$N_C = N_1 - A_C + \frac{N_2}{2} + \frac{N_3}{3} + \ldots$$

is the integrated area of a given line in the one fold spectrum corrected for accidentals, A_C, and for the effect of higher order coincidences.[4] N_S is the integrated area of the same line in the "singles" spectrum. The total efficiency times solid angle was measured to be $\frac{\varepsilon\Omega}{4\pi} = 0.084 \pm 0.003$. If gammas are detected in two or more detectors within resolving time τ, approximately 200ns, they were recorded as a coincidence. Table I lists the measured α-ray multiplicities for some well known transitions in the various residues from the $^{16}O + ^{12}C$ reaction. Note the general rising trend in multiplicity with increasing energy as the higher levels are populated. The uncertainty listed includes the effect of the residual energy dependence of $\varepsilon\Omega$.

TABLE 1

$^{16}O + ^{12}C$ Gamma Ray Multiplicities

Residue	Transition Energy (KeV)	^{16}O Beam Energy (MeV) 43.2	46.0	48.3	50.8	53.7	56.0	60.7
^{23}Na	(440)	2.07	2.32	2.37	2.66	2.60	2.79	2.95
	(627)	3.10	3.34	3.30	3.62	3.54	3.59	3.75
	(2264)	2.53	2.58	2.57	2.84	2.73	2.92	2.95
^{20}Ne	(1634)	1.73	1.88	1.86	2.00	1.99	2.12	2.17
	(2613)	1.94	2.06	2.11	2.07	2.00	2.12	2.00
^{26}Al	(417)	2.41	2.47	2.61	2.75	2.80	2.89	3.02
	(830)	2.89	3.15	2.96	3.30	3.02	3.13	3.13
	(1004)	3.23	3.32	3.31	3.37	3.65	3.70	3.26
^{26}Mg	(1130)	4.06	3.40	4.12	3.77	3.57	3.61	3.50
	(1809)	2.84	2.98	3.04	3.47	3.21	3.07	3.38
	(2511)	2.97	2.90*	3.39*	3.02*	4.10*	3.05*	4.20*
^{24}Mg	(1368)	2.95	3.07	3.08	3.28	3.09	3.17	3.31
	(2754)	3.34	3.39	3.07	3.05*	3.34*	3.23*	3.21*
	(3509)	2.50*	2.42*	2.70*	2.56*	3.33*	3.16*	3.37*

ALL VALUES HAVE UNCERTAINTIES LESS THAN 8% EXCEPT THOSE INDICATED BY ASTERISK, THEY HAVE UNCERTAINTIES LESS THAN 13%.

In the average α-ray energy measurement, a Ge(Li) detector was placed at an angle of -55° relative to the beam. A NaI detector, 9" in diameter by 4", was placed at an angle of 55° and was shielded by a 3 in thick lead collimator with a conical aperture of half angle 20.5°. Each accepted coincident event consisted of pulse heights for the Ge(Li), the NaI, and a TAC, and runs were made at the same seven beam energies as in the multiplicity experiment. Fig. 1a shows the complete Ge(Li) spectrum for 50.8 MeV, where several important transitions are identified. The analysis of the NaI spectra in coincidence with various Ge(Li) lines is in progress.

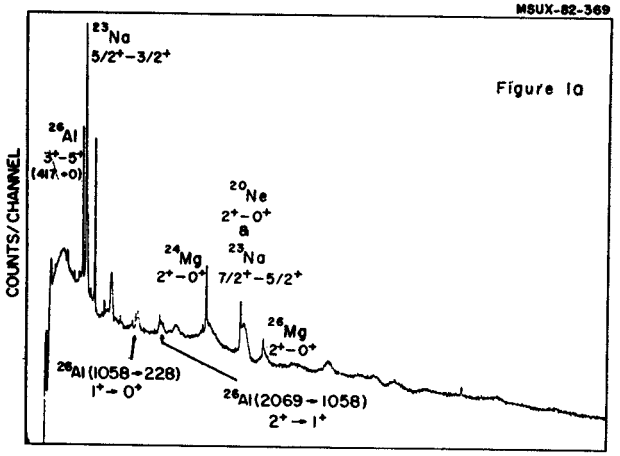

Fig. 1a. Open Ge(Li) spectrum for 50.8 MeV ^{16}O incident on ^{12}C.

The third step of the experiment was to measure the neutron energy spectra at the same seven beam energies. Six 5 in diameter by 3 in neutron detectors were arranged at various angles about the target, four in the plane (of the beam and Ge(Li) detector at $\pm$ 125°) and two out of the plane. Events were digitized and recorded on magnetic tape for each energy only for coincidences with the Ge(Li) detector. The analysis of the data is currently being carried out; a Ge(Li) spectrum gated on a neutron event in any one of the six neutron detectors for E_{lab} (^{16}O) = 50.8 MeV is presented as Fig. 1b. In comparing

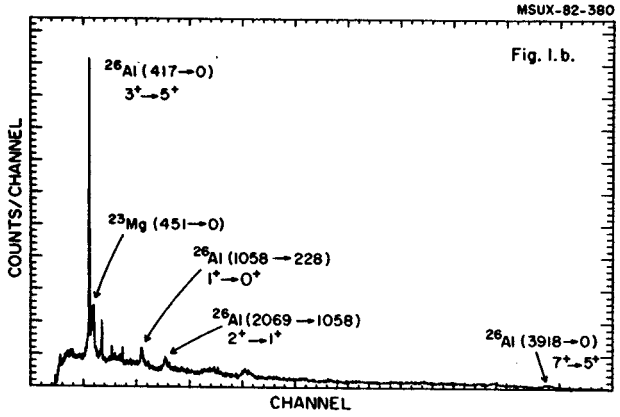

Fig. 1b. Neutron-gated Ge(Li) spectrum for above beam and target.

with Fig. 1a, a α-gated Ge(Li) spectrum, the salient feature is the enormous enhancement of α peaks from residual nuclei resulting from neutron channel decays of $^{28}Si^*$. In particular, note the relative magnitude of the ^{26}Al 417 keV ($3^+ \rightarrow 5^+$) peak in Fig. 1a and Fig. 1b. The branch $^{26}Al^*+p+n$ is by far the dominant neutron channel for the decay of $^{28}Si^*$ for all but the highest beam energies.

The final phase of the experiment is the charged particle detection. A single charged particle telescope was set at 30° and then at 45° for each energy, allowing identification of the particle type and determination of its energy spectrum. The analysis of these data is just beginning, but preliminary plots of E vs E (see Fig. 2) separate the charged particles by type and show a surprisingly large number of deuterons. Additional data will be taken at a smaller angle.

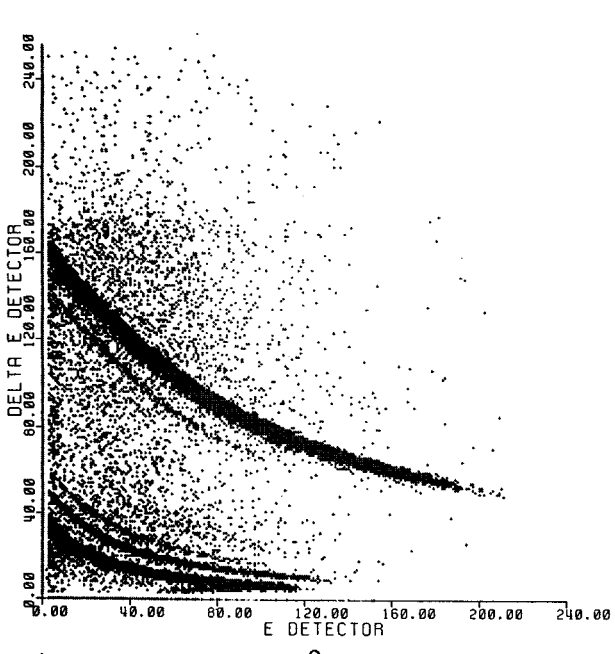

Fig. 2. ΔE vs. E at 45° to a beam of 60.7 MeV ^{16}O incident upon ^{12}C.

---

* University of Notre Dame

** University of Kansas

1. J.J. Kolata, R.M. Freeman, F. Haas, B. Heusch, and A. Gallman, Phys. Lett. 65B (1976) 333.
2. J.J. Kolata, Phys. Lett. 95B (1980) 215.
3. P. Sperr, S. Vigdor, V. Eisen, W. Henning, D.G. Kovar, T.R. Ophel and B. Zeidmann, Phys. Rev. Lett. 36 (1976) 405.
4. G.B. Hagemann, R. Broda, B. Herskind, M. Ishihara, and S. Ogaza, Nucl. Phys. A245 (1975) 166.

Angular Momentum Dependence of Neutron Spectra in the 245 MeV ^{64}Ni + ^{92}Zr Reaction

W. Kuhn*, I. Ahmad*, P. Chowdhury*, R.V.F. Janssens*, T.L. Khoo*, F. Haas, J. Kasagi, and R.M. Ronningen

Neutron spectra in coincidence with the gamma ray sum energy have been measured in the ^{64}Ni + ^{92}Zr reaction, using a 245 MeV Ni beam from the Argonne National Laboratory superconducting linac. Time-of-flight and pulse shape discrimination techniques were employed to identify the neutrons and a 33 cm x 30 cm NaI detector was used to measure the gamma sum-energy.

The compound nucleus ^{156}Er is produced at relatively low excitation energy (52 MeV) and its decay is dominated by the 2n channel. This accentuates the angular momentum dependence of the neutron spectra. Fig. 1 shows neutron spectra for different sum energy slices (i.e., spin slices). We observe that the spectra coincident with higher gamma sum-energies, corresponding to the decay of higher angular momentum states, are characterized by lower temperatures. Presumably, this reflects the fact that the excitation energy above the compound nucleus yrast line decreases with ℓ.

* Argonne National Laboratory

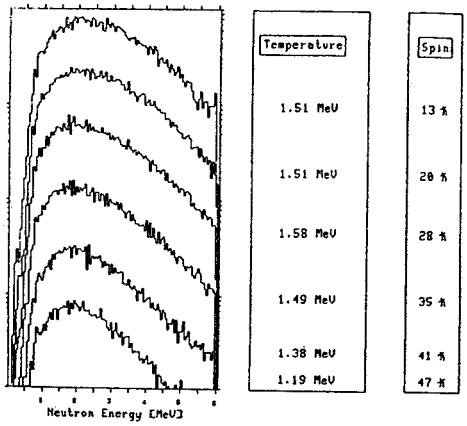

Fig 1. Neutron energy spectra (in the center-of-mass system) for different γ-ray sum-energy slices. Each slice corresponds to an average entry line spin value, deduced from the γ multiplicity as a function of the sum energy. The spectra exhibit lower temperatures for higher spins.

Fission Following Capture Reactions of $^{32}S + ^{208}Pb$

M.B. Tsang, D. Ardouin, B.B. Beck[+], P.A. Baisden[++], R. Betts[+], C.K. Gelbke, W.G. Lynch, M.S. McMahan[++], S. Saini[+], and Z. Xu

Recent measurements on the increase in the FWHM of the fission fragment mass distributions as a function of maximum entrance channel angular momentum (ℓ_{crit}) have been interpreted as a signature of a new type of reaction mechanism called "fast fission"[1]. This process is predicted to be important for entrance channel angular momenta exceeding the value $\ell_{Bf=0}$ corresponding to zero liquid drop model fission barrier of the compound nucleus. For these angular momenta, a true compound nucleus cannot be formed. In addition to the mass widths, the investigation of fission fragment angular distribution provides useful information about the onset of fast fission processes. Recent angular distribution measurements[2] of $^{32}S+^{197}Au$, ^{232}Th, ^{238}U, and ^{248}Cm have indicated that the saddle points of the composite systems are significantly more deformed than predicted by the rotating liquid drop model. To systematically investigate the possible transition from normal fission to fast fission, we have measured the angular distributions and mass widths of fission fragments from the $^{32}S+^{208}Pb$ reaction between 180 and 266 MeV. The experiments were performed at the Argonne National Laboratory Superconducting Linac.

(I) Fission Fragment Mass Widths

The experimental set up is shown in Fig. 1. Fission fragment mass distributions were obtained with standard time-of-flight (TOF) technique using the system labelled TOF in Fig. 1. The start signal was obtained from the RF of the Tandem linac while the stop signal came from a channel plate detector placed at 15.4 cm from the target. A Si detector placed behind the channel plate detector supplied the energy information. The timing signals from the channel plate detector have the advantage that they are not subject to the plasma delays one observes for timing with stop signals derived from Si detectors.[3] We also measured the relative time between the E-Detector and the RF of the Tandem Linac. Due to short separation of the adjacent RF pulses (20.6 ns) this additional time information is necessary for good background reduction. Neutron corrected mass spectra in the rest frame of the composite system obtained at 180, 210, 250 and 266 MeV respectively are compared in Fig. 2a. In Fig. 2b, the FWHMs are plotted as a function of ℓ_{crit} obtained from the angular distribution as discussed below. An increase of 14.5 amu was observed over the range of ℓ_{crit}=31h to ℓ_{crit}=104h.

The angular dependence of the mass widths at 180, 250, and 266 MeV was investigated and found to be constant within our experimental accuracy over the range of θ_{lab}=40° to 110°.

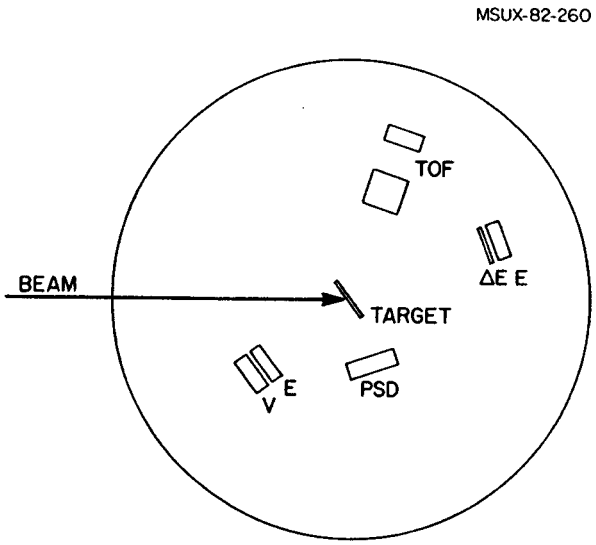

Fig. 1. Experimental set up.

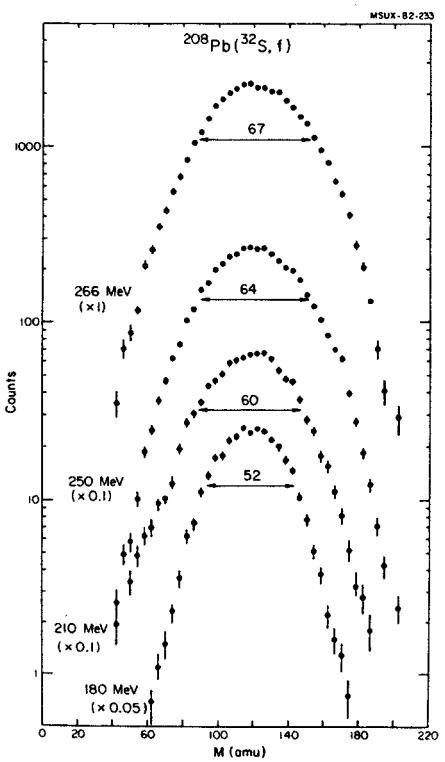

Fig. 2a. Neutron corrected mass width in the center of mass systems for E_{lab}=180,210,250 and 260 MeV.

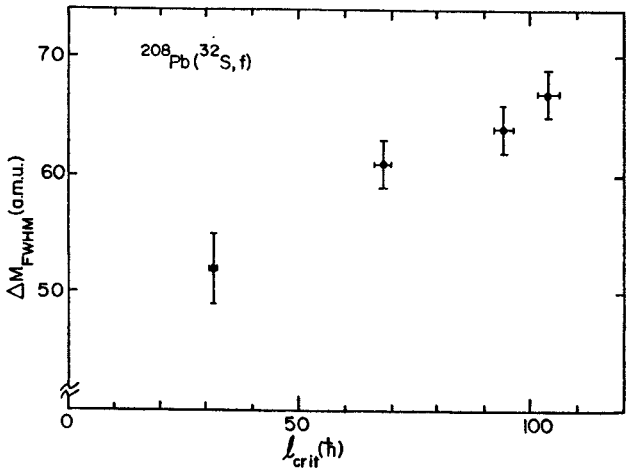

Fig. 2b. FWHM of the mass spectra as a function of ℓ_{crit}.

This seems to indicate either that "fast fission" occurs on a time scale long compared to the orbital period of the confined system or that mass equilibration is achieved before the occurrence of fission.

(II) Sequential Fission Fragments

To estimate the contribution from fission fragments arising from excited target-like fragments, fission fragment folding angle distributions were measured by detecting complementary fission fragments with a position sensitive detector (PSD) placed in the opposition side of the beam from the TOF telescope as shown in Fig. 1. The TOF telescope was moved from 60° to 85° degrees while the PSD (subtending an in-plane angle of 30 degrees) was moved from 70° to 90°. The measured peak positions of the folding angle distributions are shown in Fig. 3. For comparison, folding angles predicted for complete ($\Delta p/p=1$), and incomplete ($\Delta p/p=.9$ and $\Delta p/p=.8$) linear momentum transfer are included in the figure. Within the accuracy of the angular calibration of the folding angle distribution ($\Delta\theta\sim3^{o}$) the majority of the events are consistent with full linear momentum transfer as expected from complete fusion. (Alternatively, the measured peak position corresponds to momentum transfer of more than 90% of the projectile momentum. Note that incomplete fusion is not expected to occur at the lower energy of 180 MeV.) At forward angles, ($\theta_{lab}<90^{o}$), sequential fission following inelastic scattering and multi-nucleon transfer reactions is kinematically separated from the fusion fission fragment. The contribution from sequential fission is estimated to be less than 5% of the fusion fission fragment cross-section.

MSUX-82-174

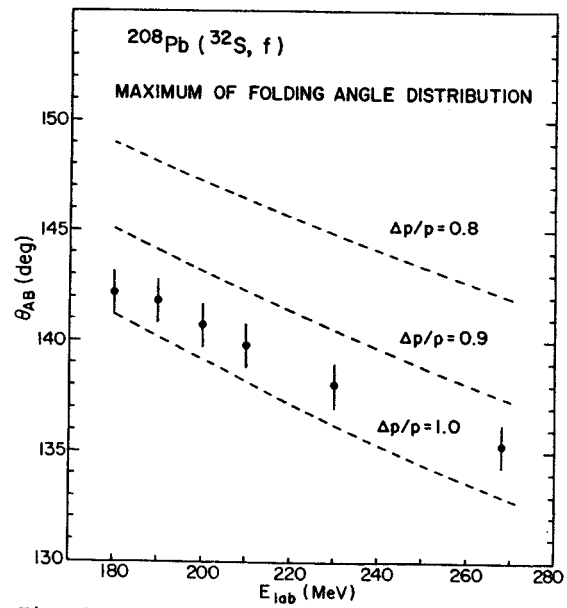

Fig. 3. Fission fragment folding angle as a function of E_{lab}.

(III) Angular Distributions

For the measurements of the angular distributions, fission fragments were identified with time-of-flight and DE-E telescope technique at forward angles and by simple time-of-flight measurements at backward angles. The start signals were derived from the Linac RF. To reduce the background from light particles such as alphas and protons, a thin (30 μm) E detector backed by a 150 m veto detector was used at backward angles. These two detector systems are labelled as DE-E and EV in Fig. 1 respectively. The angular distributions for fusion-fission fragments obtained for 180, 210, 250 and 266 MeV are shown in Fig. 4. The angular distributions deviate from $1/\sin(\theta)$ (the dash-dot curve in Fig. 4). The angular distribution of $1/\sin$

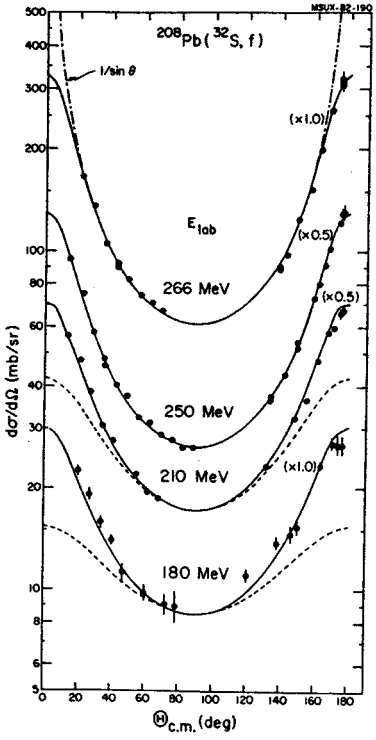

Fig. 4. Angular distribution for E_{lab}=180,210, 250 and 266 MeV. The solid lines are the best fit dashed curves for 180 and 210 MeV are liquid drop model predictions and dash-dot curve is 1/2 in θ function normalized at 90°.

is expected if the fragments are emitted isotropically in the plane perpendicular to the axis of rotation. For the two lowest energies a significant part of the fission cross section corresponds to angular momenta of non-vanishing liquid drop fission barrier. For these cases, the dashed curves show the predicted angular anisotropies using average moments of inertia as predicted by the rotating liquid drop model. The predicted angular anisotropies are significantly smaller than observed experimentally. This fact has been taken as evidence for the occurrence of fast fission.

$$\frac{d\sigma^{fission}}{d\Omega}(\theta) = \sum_{\ell=0}^{\infty} W_\ell(\theta)\,(\sigma_\ell^{fusion} \cdot P_\ell^{fission})$$

where σ^{fusion} and $P_\ell^{fission}$ are the partial wave function cross section and the corresponding fusion probability after compound nucleus formation. The angular distribution of fission fragments can be described by

$$W(\theta) = \frac{\sum_{K=\ell}^{\ell} \frac{1}{2}(2\ell+1)\,|D^{\ell}_{M=0,K}(\theta)|^2 \exp(-K^2/2K_o^2)}{\sum_{K=-\ell}^{\ell} \exp(-K^2/2K_o^2)}$$

where

$$K_o^2 = (T/\hbar^2)\, i_{eff}\,, \quad \frac{1}{i_{eff}} = \frac{1}{i_{\parallel}} - \frac{1}{i_{\perp}}$$

The values of i_{sph}/i_{eff} used were 2.718, 1.097, 0.861, and 0.91 (in the calculations at 180, 210, 250 and 266 MeV, respectively. Note that for two touching spheres of equal size one has $i_{sph}/i_{eff}=1.13$ and for a spherical saddle point $i_{sph}/i_{eff}=0$.

The total fission fragment cross-sections are plotted as a function of incident energies in Fig. 5. The dashed curve is obtained by calculating the fusion cross-section assuming penetration through a parabolic fusion barrier.[4] The dot-dashed curve corresponds to the fusion cross section calculated from the one-dimensional proximity model plus one body dissipation.[5] This latter calculation agrees with the data quite well. The solid curve corresponds to the passage of the conditional saddle point within the framework of Swiatecki's extra-push model. At higher energies, model underpredicts the cross sections.

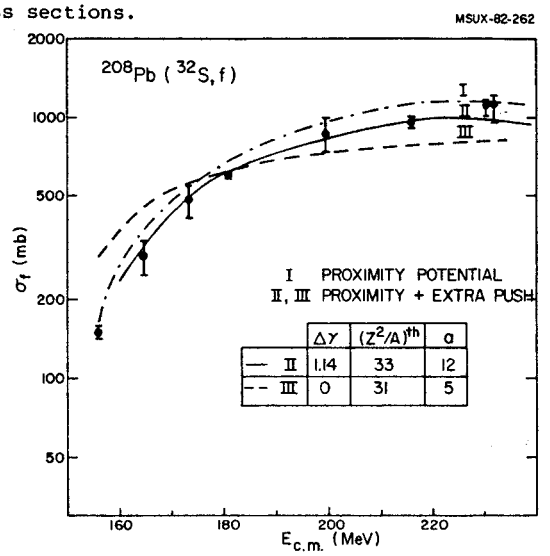

Fig. 5. Fission fragment excitation function. See text for the calculation curves.

+ Chemistry Division, Argonne National Laboratory, Argonne, IL 60439.
++ Chemistry Division, Lawrence Livermore National Laboratory, Livermore, CA 94550.

1. Borderie et al., Z. Phys. A 299, (1981) 263.
2. B.B. Back et al., Phys. Rev. Lett. 46 (1981) 1068.
3. H. Henschel et al., Nucl. Inst. Meth., 125 (1975) 365.
4. C.Y. Wong, Phys. Rev. Lett. 31 (1973) 766.
5. J.R. Birkelund et al., Phys. Rep. 56, (1979) 107.
6. W.J. Swiatecki, Nucl. Phys. A376 (1982) 275.

Sequential Fission in the Reaction of $^{40}Ar + ^{197}Au$

D.J. Morrissey, G.J. Wozniak[+], L.G. Sobotka[+], A.J. Pacheco[+], R.J. McDonald[+] and L.G. Moretto[+]

The measurement of particle and α-ray angular distributions associated with deep-inelastic collisions (DIC) allows one to study the process of angular momentum transfer through the determination of the magnitude and alignment of the fragment spins. Large intrinsic spins can be introduced in the reaction products through the dissipation of entrance-channel orbital angular momentum. From mechanical considerations and from the rigid rotation limit, the fragments' spins are expected to be aligned perpendicular to the reaction plane. Misalignment of the fragments' spins occurs when in-plane components of angular momentum are present. These components can be generated either directly by some feature of the reaction mechanism, or by nonequilibrium or equilibrium statistical fluctuations in the angular-momentum-bearing modes of the dinuclear system. The angular distributions of sequential fission fragments are quite sensitive to the direction of the spin vector in that it can produce a substantial in-plane anisotropy. In-plane measurements of sequential fission angular distributions[1,2] have given detailed results on the magnitude and direction of the spin vector of one of the fragments from deep inelastic collisions.

A beam of 340 MeV ^{40}Ar was obtained from the Super HILAC at the Lawrence Berkeley Laboratory. This beam irradiated a metallic gold foil, approximately 1 mg/cm^2 thick. The experiment consisted of measurements of coincidences between projectile-like fragments and fission fragments. Projectile-like fragments (PLF) were detected in a gas ionization telescope that was fixed at 40° to the beam. The resolution of the Z-telescope was sufficient to completely separate atomic numbers between 6 and 36; however, it was insufficient to resolve the individual atomic numbers of the fission fragments. Fission fragments (FF) were observed on the opposite side of the beam from the PLF in an array of 10 silicon surface-barrier detectors. The array of FF detectors was positioned at various angles in order to cover as large an angular range as possible. After the experiment the data were transformed into the calculated rest frame of the recoiling target nucleus event by event. The energy and angular distributions of the FF were then available as a function of PLF energy and Z.

The fission probability of the heavy partner is shown as a function of PLF nuclear charge after integration over PLF kinetic energy in Fig. 1. The sharp minimum at Z=18 indicates the low fission-ability of gold nuclei produced

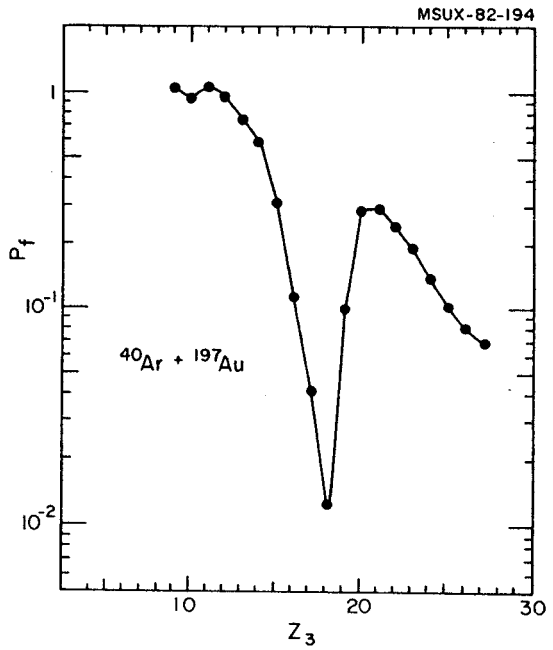

Fig. 1. The fission probability as a function of projectile-like fragment Z integrated over energy is shown.

in quasielastic collisions. The expected trend of increasing fission-ability with increasing fragment mass (i.e. decreasing PLF charge) is also seen In Fig. 1. The in-plane angular distribution of FF in the rest frame of the target nucleus is shown in Fig. 2. The data show a strong in-plane anisotropy (1.5:1) as does the fitted angular distribution function shown by the solid curve.

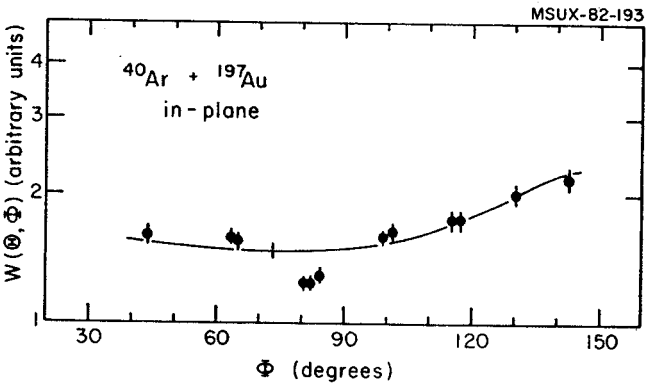

Fig. 2. The angular distribution of sequential fission fragments from the reaction of $^{40}Ar + ^{197}Au$ is shown. This angular distribution shows a significant anisotropy in the rest frame of the recoiling nucleus indicating a preferential direction for the fragment angular momentum.

+ Permanent address: Lawrence Berkeley Lab, Berkeley, CA

1. D.J. Morrissey et al., Z. Phys. A305 (1982) 131.
2. R.J. Puigh et al., Phys. Lett A336 (1980) 279.

Linear Momentum Transfer in Non-relativistic Nucleus-Nucleus Collisions

V.E. Viola, Jr.[+], T.C. Awes, B.B. Back,[++] H. Breuer,[+++] C.K. Gelbke, and K.L. Wolf[++]

A useful overview of the global features of non-relativistic nucleus-nucleus collisions can be obtained from studies of the linear momentum transfer distributions which characterize the target projectile interaction. For reactions involving highly fissionable target nuclei, where essentially the total reaction cross section leads to fission, the information about the linear momentum transfer is obtained from measurements of the folding angle distribution of the two coincident fission products.[1-5] If no momentum is transfered to the target nucleus, the two fission fragments emerge colinearly in the laboratory corresponding to a folding angle of $\Theta_{AB}=180^{o}$. With increasing recoil velocity of the target residue, the fission fragments are kinematically focused into the forward direction, resulting in folding angles $\Theta_{AB}\approx 180^{o}$.

Fig. 1 shows the in-plane folding angle distributions measured[1-5] for the system ^{16}O + ^{238}U for several bombarding energies between 110 and 315 MeV. Except for the lowest energy, two components are apparent in the data. The major fraction of the cross section is concentrated in a well defined peak corresponding approximately to complete linear momentum transfer as it is expected for fusion and fusion-like reactions. For orientation, the most probable folding angles that would be expected from the fission decay of the compound nucleus, corresponding to full linear momentum transfer, are indicated by the arrows in the figure. The second component in the folding angle distributions appears at folding angles Θ_{AB} slightly smaller than 180^{o}, where one observes a systematic growth of a broad distribution of relatively low momentum trasfer events.

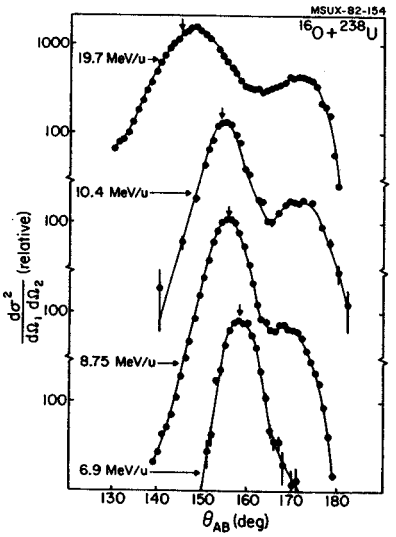

Fig. 1

At the lowest bombarding energies, the folding angle distributions are consistent with the assumption that the large momentum transfer events result from fission of the compound nucleus. With increasing beam energy, however, the maxima of the fusion-like component correspond to linear momentum transfers that are slightly less than expected from complete fusion reactions indicating the increasing importance of incomplete fusion reactions or non-equilibrium light particle emission.[3-5] Similar trends have been observed for reactions induced by α-particles, ^{12}C, ^{14}N and ^{20}Ne ions.[6]

The maxima of the folding angle distributions correspond to most probable linear momentum transfers, Δp, observed in fusion-like reactions. When expressed in units of the projectile momentum, p, the most probable linear momentum transfer appears to depend mainly on the beam velocity. Fig. 2 shows a summary of published data;[6] here the fractional, most probable linear momentum transfer, $\Delta p/p$ is plotted vs. the square root of the incident energy per nucleon (which is proportional to the beam velocity). At energies below approximately 10 MeV per nucleon, complete fusion corresponding to $\Delta p/p=1.0$ is observed. At higher energies, incomplete fusion processes become increasingly important and an approximately linear decrease of $\Delta p/p$ with beam velocity is observed. From these data little dependence on the mass of the projectile is observed. Further investigations extending to higher beam energies and using different projectiles will be necessary to investigate whether the trends observed in Fig. 2 are a universal feature of heavy ion reactions at energies above 10 MeV per nucleon.

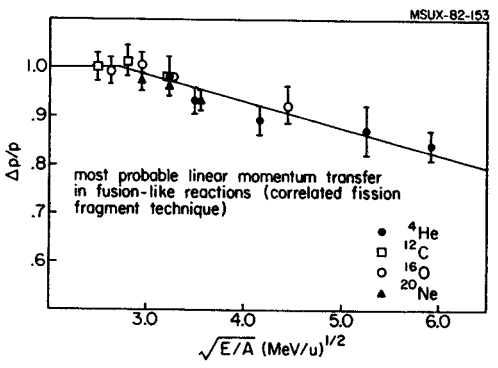

Fig. 2

+ Department of Chemistry, Indiana University, Bloomington, IN 47405

++ Chemistry Division, Argonne National Laboratory, Argonne, IL 60439

+++ Department of Physics, University of Maryland, College Park, MD 20742

1. T. Sikkeland, E.L. Haines, and V.E. Viola, Jr., Phys. Rev. 125, 1350 (1962).

2. T. Sikkeland and V.E. Viola, Jr., Proc. 3rd Conf. on Reactions between Complex Nuclei (University of California Press, 1963) p. 232.

3. B.B. Back, K.L. Wolf, A.C. Mignerey, C.K. Gelbke, T.C. Awes, H. Breuer, V.E. Viola, Jr., and P. Dyer, Phys. Rev. C22 (1980)1927.

4. T.C. Awes, G. Poggi, C.K. Gelbke, B.B. Back, B.G. Glagola, H. Breuer and V.E. Viola, Jr., Phys. Rev. C24 (1981) 89.

5. T.C. Awes, Ph.D. Thesis, Michigan State University, 1981 (unpublished).

6. For references, see: V.E. Viola, Jr., B.B. Back, K.L. Wolf, T.C. Awes, C.K. Gelbke and H. Breuer, to be published in Phys. Rev. C26.

Energy Dependence of Nuclear Matter Disassembly in Heavy Ion Collisions

B.V. Jacak, G.D. Westfall, N. Anantaraman, M.W. Curtin, G.M. Crawley, C.K. Gelbke, B. Hasselquist, W.G. Lynch, D.K. Scott, M.B. Tsang, M.J. Murphy, T.J.M. Symons, R. Legrain and T.J. Majors

An important concept in relativistic nuclear collisions concerns the formation of an excited, localized region of participant nucleons moving with a velocity intermediate between those of the projectile and target.[1] The relative abundance of emitted light charged particles as a function of temperature in the zone is characteristic of the detailed mechanism of its disassembly.[2] Within a thermodynamic model, temperature and relative numbers of nucleons and light nuclei are predicted to vary smoothly with incident energy, whereas a hydrodynamic model,[3] incorporating compression, could lead to a discontinuity in the temperature and a sudden decrease in the production of light composite nuclei as a function of incident energy.

In this work, energy spectra and angular distributions of p, d, t, ^{3}He, and ^{4}He from ^{20}Ne + Au at incident energies of 100 and 150 MeV/nucleon were measured at the Low Energy Beam Line of the LBL Bevalac. The results for production cross sections and temperatures are combined with those extracted from previous measurements for ^{16}O or ^{20}Ne-induced interactions with heavy targets, giving a consistent picture of an intermediate velocity source with a temperature that varies smoothly with incident energy.

In order to isolate the component of the particle spectra originating from an intermediate velocity source, a selection criterion was established. The low energy components of the energy spectra are expected to be due to target evaporation and therefore are not described by the moving source. Projectile fragments populate forward angles near the projectile velocity. We therefore associate fragments emitted at large angles $\geq 50^\circ$ and at energies well above evaporation energies with an intermediate source. The temperatures extracted with such a single moving source parameterization are shown in Fig. 1.

The production cross sections shown in Fig. 2 correspond to particles produced in the intermediate velocity source and are model dependent. The solid lines are drawn to guide the eye. The dashed line is the prediction for producing protons from a fireball described as a free strongly-interacting gas in thermal and chemical equilibrium at an excitation and velocity determined at the most probable impact parameter. At low incident energies the production cross sections are overpredicted by almost two orders of magnitude, since at these energies the excitation energy available is insufficient to unbind all the participant nucleons. Consequently,

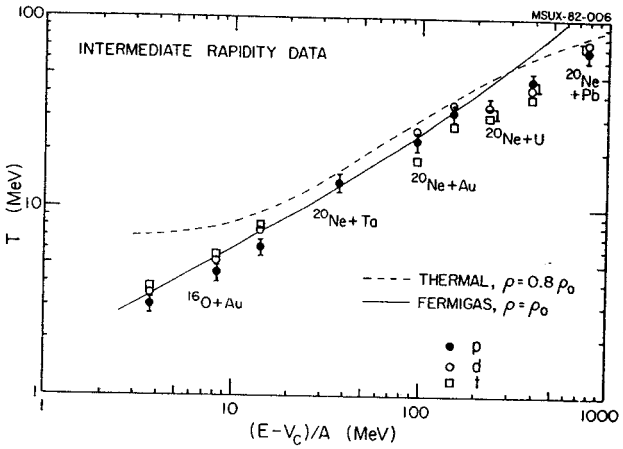

Fig. 1. Temperatures extracted with a single moving source parameterization for p, d and t as a function of bombarding energy above the Coulomb barrier.

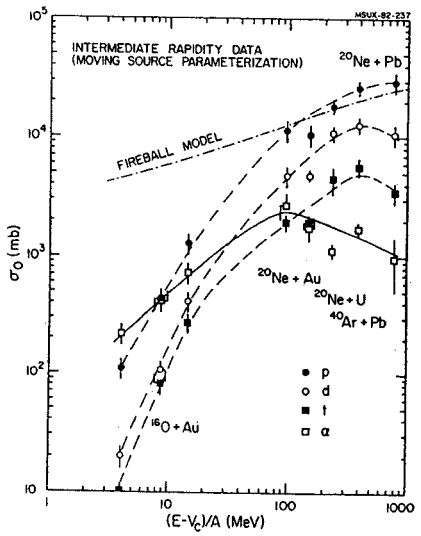

Fig. 2. Integrated production cross sections for midrapity particles as a function of bombarding energy above the Coulomb barrier. These cross sections are the integration of the moving source spectra, and exclude contributions from projectile-like and target-like sources.

only a fraction of the particles in the overlap region are emitted.

In Fig. 3 the cross sections for particles obtained from the fits to the intermediate source are shown as ratios of composites (d, t, ^{4}He) to protons. These ratios exhibit a striking behavior in that the d/p and t/p ratios are nearly

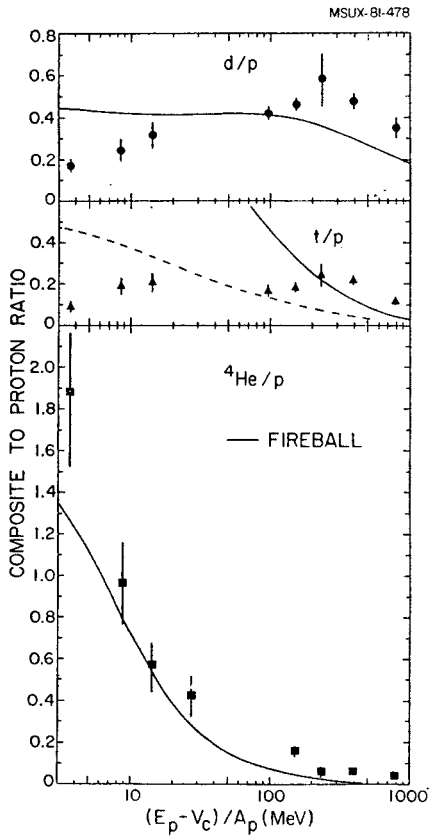

Fig. 3. Ratios of production cross sections of composite particles to protons. The solid lines are predictions of the Fireball model, and the dashed line is the prediction of the Fireball model, and the dashed line is the prediction of the Fireball model without decay of nuclear resonances.

constant with energy, whereas the ^{4}He/p ratio drops drastically with increasing projectile energy. The solid lines correspond to predictions using the fireball model as above. The decay of nuclear resonances is an essential ingredient in the calculation and accounts for the observed constancy of the d/p ratio. The success of the thermal model in reproducing the constant d/p ratio casts doubt on the interpretations of Ref. 4, where the d/p ratio was related directly to the entropy produced in heavy ion collisions.

The observed decrease of the ^{4}He production compared to protons is a striking observation consistent with thermal, explosion models. Our results emphasize the importance of measuring light composite fragments as well as nucleons to study the properties of hot, dense nuclear matter.

---

1. G.D. Westfall, J. Gosset, P.J. Johansen, A.M. Poskanzer, W.G. Meyer, H.H. Gutbrod, A. Sandoval, and R. Stock, Phys. Rev. Lett. 37 (1976) 1202.
2. J. Randrup and S. Koonin, Nucl. Phys. A356 (1981) 223; G. Fai and J. Randrup, LBL Preprint 13357 (1981).
3. S.I.A. Garpman, S.K. Samaddar, D. Sperber, and M. Zielinska-Pfabe, Phys. Lett. 92B (1980) 56.
4. P.J. Siemens and J.I. Kapusta, Phys. Rev. Lett. 43 (1979) 1486.

Composite Fragment Production in Intermediate Energy Heavy Ion Reactions

B.V. Jacak, C.K. Gelbke, L.H. Harwood, W.G. Lynch, D.K. Scott, T.J.M. Symons, M.B. Tsang and G.D. Westfall

In intermediate energy heavy ion reactions, a transient nuclear system can be formed with an excitation energy comparable to its binding energy. Its subsequent decay can take place through many channels, with the formation of many composite fragments.[1] In addition to this statistical disassembly, it is possible that at a certain temperature the zone will explode, leading to an increase in the nucleon multiplicity and a drop in the mean emitted fragment mass. Light charged particle production has been studied for a broad range of bombarding energies.[2] Some data for production of composite fragments heavier than ^{4}He exist,[3] but a detailed study of these cross sections as a function of bombarding energy is necessary to understand the disassembly of the transient system.

The present work consists of single particle inclusive cross section measurements for the systems ^{40}Ar + Au and ^{40}Ar + Ca at 50, 100 and 150 MeV/nucleon. Beams of approximately 1 x 10^7 particles/second from the Low Energy Beam Line of the LBL Bevalac were used. Energy spectra and angular distributions were determined for midrapidity lithium, beryllium, boron and carbon using stacks of silicon detectors. The energy spectra and angular distributions of p, d, t, ^{3}He and ^{4}He were measured as well with a telescope consisting of two thin silicon detectors followed by a four-inch thick NaI detector. The angular distributions cover the range between 30° and 130°.

Targets consisted of 80 mg/cm^2 and 200 mg/cm^2 Au and 35 mg/cm^2 and 160 mg/cm^2 Ca, mounted at 45° to the beam. The telescopes were calibrated using direct beams of 150 MeV/nucleon p, ^{4}He and ^{20}Ne, degraded to five energies between 130 and 30 MeV/nucleon. For elements from hydrogen through boron, isotopes were well resolved by the detector telescopes.

The energy spectra of midrapidity lithium isotopes from ^{40}Ar + Au at 150 MeV/nucleon are shown in Fig. 1. The solid lines are the results of a fit to the data with a single moving source model. Such a single moving source at approximately half the beam velocity can be expected to fit most of the data, with the exception of forward angles and low energies due to contributions from projectile-like and target-like sources. The experimental cutoffs for the lithium isotopes were such that all the data were used in making the fits. The extracted source temperatures and velocities are very similar to the temperatures and velocities obtained by fitting the light charged particle data (p,d,t,^{3}He, and ^{4}He) with the same model. This result lends credence to the idea that the composite fragments and light charged particles arise from a similar mechanism.

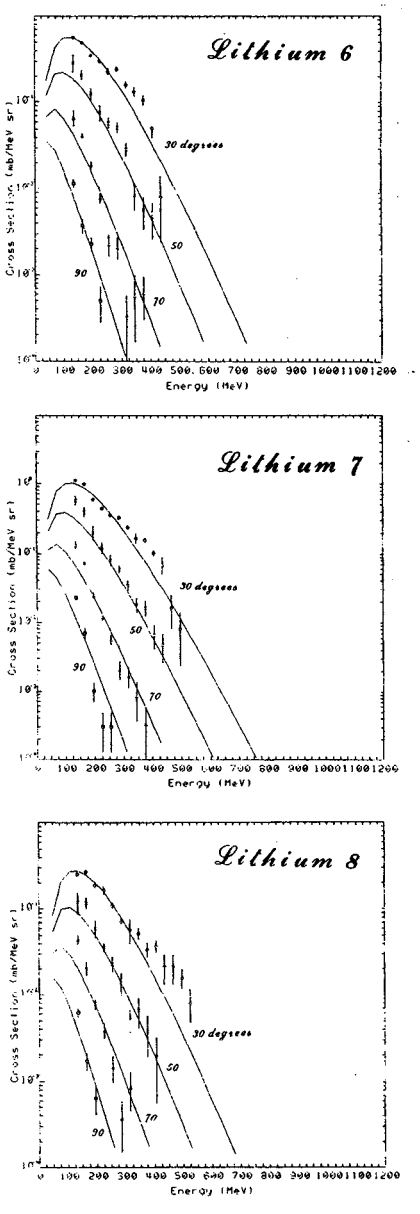

Fig. 1. Spectra of midrapidity Lithium isotopes from 150 MeV/n Ar+Au. The solid lines are fits with a single moving source. The spectra for each isotope are fitted separately.

The data for the heavier fragments will similarly be fitted with a single moving source and the extracted parameters examined for consistency with the source giving rise to lighter particles. The integrated cross sections for midrapidity products will be used to extend the

measurement of relative production of fragments as a function of mass. The data for the remainder of the bombarding energies and targets will be similarly analyzed to yield systematic information about the mechanism for producing composite fragments.

---

1. J. Randrup and S.E. Koonin, Nucl. Phys. A356 (1981) 223; G. Fai and J. Randrup, LBL Preprint 13357 (1981).
2. G.D. Westfall, B.V. Jacak, N. Anantaraman, M.W. Curtin, G.M. Crawley, C.K. Gelbke, B. Hasselquist, W.G. Lynch, D.K. Scott, B.M. Tsang, M.J. Murphy, T.J.M. Symons, R. Legrain, and T.J. Majors, Phys. Lett. 116B (1982) 118.
3. J. Gosset, H.H. Gutbrod, W.G. Meyer, A.M. Poskanzer, A. Sandoval, R. Stock and G.D. Westfall, Phys. Rev. C16 (1977) 629; K.A. Frankel and J.D. Stevenson, Phys. Rev. C23 (1981) 1511.

Liquid-Gas Phase Instabilities in Nuclear Systems

M.W. Curtin, H. Toki and D.K. Scott

To derive the condition for a liquid-gas instability, we start from the relation[1]

$$\rho = \frac{4}{(2\pi)^3} \int d^3k [1 + \exp\ (\frac{k^2}{2m} - \mu)/T]^{-1}$$

from which the chemical potential, μ, is determined as a function of the density ρ and the temperature T. The thermal contribution to the internal energy is given by

$$\frac{E_T}{V} = \frac{4}{(2\pi)^3} \int d^3k\ \frac{k^2}{2m} [1 + \exp\ (\frac{k^2}{2m} - \mu)/T]^{-1}$$

using the calculated values of μ. The pressure due to the thermal motion is then $2E_T/3V$ corresponding to a zero point pressure of $\frac{2}{5}\ \varepsilon_F(\rho)$ where ε_F is the Fermi Energy. The total pressure is the sum of the thermal pressure and the pressure, P_V due to the interaction among the constituents of the system. To derive P_V we express the energy per nucleon in the form[2] obtained from a Skyrme type interaction

$$\frac{E_V}{A} = - A\rho + B\rho^{\sigma+1}$$

where A and B are constants determined by the constraint E/A = -16 MeV (for nuclear matter) when $\rho = \rho_o$ together with the further condition for stability of normal density nuclear matter, $\partial(E/A)/\partial\rho = 0$.

Solving for A and B with $\varepsilon_F(\rho = \rho_o) = 38$ MeV and $\sigma = 2/3$ we find $A\rho_o = 74.2$ MeV and $B\rho_o^{5/3} = 35.4$ MeV. In general A and B have some temperature dependence but here we assume that the thermal and interaction energies and pressures are separable. The pressure due to the interaction (at T=0) is $\rho^2\ \partial(E/A)/\partial\rho$, resulting in

$$\frac{P_V}{\rho} = - A\rho + \frac{5}{3} B\rho^{5/3}$$

The total pressure as a function of density for constant temperature is plotted in Fig. 1, which shows that the equation of state has the form typical of a Van der Waal's system with liquid and gaseous phases. For the unphysical region (shown only for T=15 MeV) where the slope is negative (implying a negative incompressibility) a Maxwellian construction is employed, along which the liquid and gas phases coexist. The region of coexistence is indicated in the figure. The range of densities compatible with coexistence becomes smaller as the temperature increases until the apex of the coexistence region coincides with the inflection point of the critical temperature curve. At this critical temperature

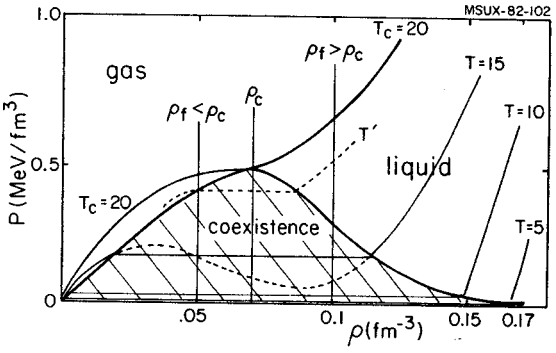

Fig. 1. Pressure versus density for fixed temperature is plotted. Solid curves indicate paths traversed by a system with fixed T. Liquid, gas and coexistence (hatched) regions are indicated. The significance of ρ_f, ρ_c are discussed in the text.

$T_c \tilde{=} 20$ MeV the co-existence of liquid and gas phases is possibly only at $\rho_c \cong 0.07$ fm^{-3} and only a gaseous phase exists for all higher temperatures. Our results are in good agreement with recent calculations.[3]

Our choice of parameters leads to an incompressibility of 310 MeV.[4] Current estimates from nuclear monopole excitations indicate that the incompressibility is 210 MeV.[5] In our calculation we let E/A = -16 MeV (ignoring surface effects) and $\sigma = 2/3$ in the Skyrme interaction. The thermodynamic treatment implies a large system and hence E/A = -16 MeV is fixed. If σ is allowed to change to reproduce K = 210 MeV, a critical temperature of 17 MeV is predicted.

We note that during the disassembly phase of the hot region, the density decreases until the thermal freeze out density (ρ_f) is reached. This density is roughly defined when the mean free path becomes commensurate with the physical size of the hot region. Collisions cease at ρ_f and the fragments travel undisturbed to the detectors aside from final state interactions.[6] To observe both liquid and gas phases at a given temperature the Maxwellian construction must encompass ρ_f. If ρ_f is large then the system will be in the liquid phase at freeze out, whereas if ρ_f is small only the gas phase will exist signifying that the system has traversed the coexistence portion of the isotherm and the liquid phase no longer exists.

In the event that $\rho_f < \rho_c$ the system will enter the gas phase prior to freeze out leading to an erroneous interpretation of T (see Fig. 1) as the critical temperature T_c. Further in-

spection of Fig. 1 indicates that for $\rho_f \geq \rho_c$ the temperature T_c will be correctly identified. The smallest value of ρ_f quoted in ref. 7 is 0.4 ρ_o ($\pm$30%) allowing us to set a lower limit on ρ_f of 0.05 fm^{-3}. As illustrated in Fig. 1 the coexistence boundary intersects this minimal ρ_f on the T $\cong$ 19 MeV isotherm, leading to an error in the determination of the critical temperature of 1 MeV. As we shall see below it is difficult to extract experimental temperatures with greater accuracy.

In a recent paper[8] the trends of emitted light particles (p,d,t,^{3}He,α) were studied. For each reaction a component in the energy spectra was attributed to emission from a localized participant source of velocity intermediate between those of projectile and target and the associated temperatures were deduced. The integrated cross-sections from the source for each particle are shown in Fig. 2. The curves are labeled by the incident energy, projectile and target on the left. Temperatures are labeled on the right. In each case a range of temperatures is indicated accommodating the limits for fitting spectra of different emitted particles.

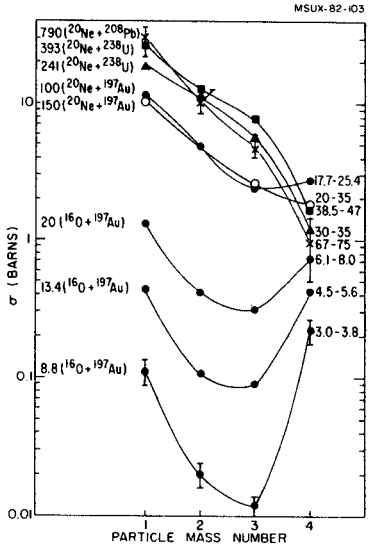

Fig. 2. Cross-sections for different fragment masses are plotted for a range of incident energies (shown on the left) and equivalent temperatures (right). Error bars are indicated for highest (X) and lowest (●) incident energies.

At high incident energies, corresponding to high temperatures, the yield falls off monotonically as a function of particle mass. This behavior is expected for emission of clusters from a high temperature single gaseous phase where the composite production cross section can be related to a power of the nucleon cross section. This result is common to both the coalescence and thermal models. In the region of $E_{inc} \cong 100$ MeV/u corresponding to T $\cong$ 20 MeV, the distribution flattens and at still lower temperatures the trend reverses so that the alpha particle yield exceeds that of lighter particles. While it is tempting to attribute this enhanced cluster formation at temperatures below 20 MeV to the onset of the liquid-gas instability we have discussed, it is necessary first to study the consequences of the large alpha binding energy in the gas model.

From the standpoint of internal energy it is very favorable to form an alpha since the binding energy per nucleon (at $\rho = \rho_o$ and T = 0) is 7.1 MeV. Since the entropy steadily decreases with increasing fragment mass, the formation of a carbon nucleus is less favored than an alpha particle although the binding energies per nucleon are comparable. The binding energy per nucleon of the alpha far exceeds any of the nearest neighbors thus making it a very favorable structure. Bearing this in mind, we construct a gas composed of alphas and nucleons. The partition function for alphas and nucleon is

$$Z = \frac{1}{N_n!}\,(4\, q_n\, V_n)^{N_n} \cdot \frac{1}{N_\alpha!}\,(q_\alpha\, V_\alpha\, e^{B/T})^{N_\alpha}$$

where $q_i = (M_i T/2\pi\hbar^2)^{3/2}$, the quantum concentrations for nucleons and alphas. The free energy is defined as $F = -T \ln Z$. Furthermore, we require $\partial F/\partial N_\alpha = 0$. To account for the hard core of the alpha we replace V_α by V'_α where $V'_\alpha = V_\alpha - N_\alpha\, v_\alpha$ and the excluded volume $v_\alpha \approx (4\pi/3)\,(2)^3$ fm^3.

The number nucleons participating in the interaction region was chosen to be 40 commensurate with the geometry of the participant zone and with experimental determinations (see ref. 10 and references therein). The ratios N_d/N_p and $(N_t + N_{^3He})/N_p$ are assumed constant and equal to 1/3 and 1/10 respectively.[9] The freeze out density was fixed at 0.05 fm^{-3}. (However, the results are not significantly different for ρ_f = 0.08 fm^{-3}.) The results of the calculation in Fig. 3 reproduce the trends of the experimental data and reinforce the idea that light particle emission has a thermal origin. It would be difficult, for example, to explain these results with a final state coalescence model. The influence of a liquid-gas phase instability may be more clearly discernable in the cross sections for heavier clusters (A>4), which are likely to be enhanced at the onset of the liquid phase but which are strongly disfavored in the simple gas model. In this context we note the recent observation in relativistic proton induced spallation of heavy targets: the yield for fragments of mass A is of the form $Y(A) \propto A^{-x}$ where $2 \leq x \leq 3$.[10] Such a power law distribution is expected of systems at the critical point for condensing to the liquid phase.[11]

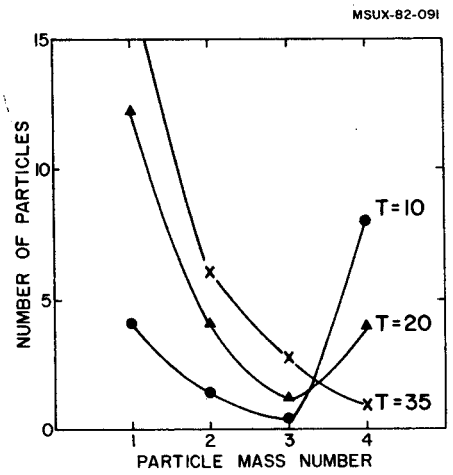

Fig. 3. The α-particle yield predicted by minimizing the free energy, keeping the ratios N_d/N_p and $(N_t+N_{^3He})/N_p$ fixed.

In this paper we have shown that a liquid-gas phase instability may develop in nuclear systems when T ≅ 20 MeV. At higher temperatures existing experimental data on light composite fragment production appear consistent with emission from a gaseous phase. The observed enhancement of alpha particles at lower temperatures cannot, at present, be unambiguously attributed to the formation of clusters expected at the onset of the liquid phase, since the large binding energy per nucleon of the alpha particle also favors its production in a single phase gas model. The influence of a liquid phase transition might be more readily observable in the production of heavier clusters which should be strongly inhibited in the non-interacting gas model.

1. C. Kittel and H. Kroemer, Thermal Physics (W.H. Freeman and Co., San Francisco, 1980).
2. L. Zamick, Phys. Lett. 45B, 313 (1973).
3. B. Friedman and V.R. Pandharipande, Nucl. Phys. A361, 502 (1981); G. Ropke, L. Munchow and H. Schulz, Preprint, 1982.
4. M.A. Preston and R.K. Bhaduri, Structure of the Nucleus (Addison-Wesley, Massachusetts, 1975).
5. F. Serr, G. Bertsch and J.P. Blaizot, Phys. Rev. 22, 922 (1980).
6. A. Mekjian and D. Gupta, Phys. Rep. 72C, 133 (1981).
7. M.C. Lemaire et al., Phys. Lett. 85B, 38 (1979).
8. G.D. Westfall et al., Michigan State University Preprint MSUCL-365 (1982).
9. S. Nagamiya et al., Phys. Rev. C 24, 971 (1981).
10. R.W. Minich et al., Purdue University Preprint, 1982.
11. M.E. Fisher, Phys. 3, 255 (1967).

Application of the Moving Source Model to α-particle Induced Reactions, and to Heavy Cluster Production

S. Angius and D.K. Scott

The high energy tails of energy spectra of light particles (p→α), emitted in heavy-ion induced reactions, are frequently described with a moving source model, parameterized by a velocity and a temperature.[1,2] At relativistic incident energies, this source is identified with the nuclear fireball, whereas at low energies a localized hot-zone may be the origin.[3] In this note we apply the same parameterization to light particle emission for α-induced reactions, as well as to the production of heavier clusters, e.g. ^{12}C and ^{11}B, in ^{40}Ar induced reactions.

The basic assumption is that a source at temperature τ and moving with velocity $\frac{v}{c}$ in the center of mass frame, is isotropically emitting particles. The energy distribution in the source is assumed to be a classical Bolztmann distribution which in the frame of the moving source, has the form:

$$\frac{d^2\sigma_s}{dE_s d\Omega} = N \sqrt{E_s}\, \exp(-E_s/\tau).$$

where E_s is the total energy of the particle.

This distribution must be transformed into the laboratory frame and a correction for the Coulomb repulsion from the source has been introduced. The Coulomb shift gives:

$$\frac{d^2}{dE_s d}\,{}_s = N \sqrt{E_s - E_c}\, M(T_s - E_c) \exp\left(\frac{-(E_s - E_c)}{\tau}\right)$$

where T_s is the kinetic energy of the particle.

The M- function represents the physical fact that no particles can be detected at infinity with energy less or equal to the Coulomb energy.

The relativistic transformation to the laboratory frame is given by the relation:

$$\frac{d^2\sigma_L}{dE_L d\Omega_L} = \frac{P_L}{P_s} \frac{d^2\sigma_s}{dE_s d\Omega_s}$$

where $P_{L(s)}$ is the momentum of the fragment in the laboratory (source) frame. Now, introducing the relation $E_s = \gamma(E_L - \frac{v}{c} P_L \cos\theta_L)$, the distribution in the laboratory is obtained in terms of measured quantities (T_L and θ_L).

The free parameters are τ, $\frac{v}{c}$ and N. This parameterization, already successful in the case of heavier projectiles, has been proven valid also in the case of α-particles, showing that some kind of thermalization occurs even when a more limited number of nucleons are involved.

In Fig. 1 the proton spectra obtained from the Ta (α,p) reaction at 180 MeV/A[4], are shown, along with the fitted curves.

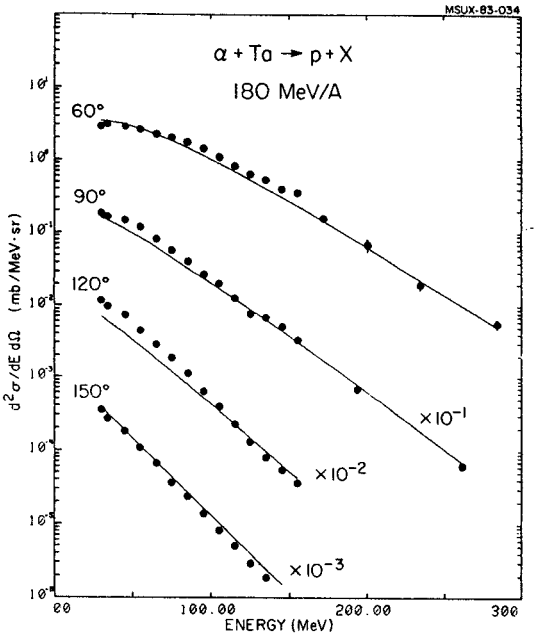

Fig. 1.

A rather good agreement is obtained also for the spectra of heavy fragments, as shown in Fig. 2, where the experimental points for ^{11}B fragment, from the Ar + U reaction[5] at 100 MeV/A are compared with the calculated curves. The reactions analyzed[4,5,6], with the relevant parameters and the final results are listed in table 1; in Fig. 3 and 4 the temperatures and velocities are plotted and compared with the values obtained for different systems. Clearly, all the points follow the same general trend, indicating that the parameterization in terms of a moving source is as valid for α-particles as it is for oxygen or neon, and that it is possible that also fragments heavier than ^4He are emitted in a similar process.

Experimental points at energies below 30 MeV and spectra taken at angles less than 60° have been excluded from this analysis, since the high yields characteristic of these regions are not accounted for by this simple parameterization. Other mechanisms of emission, such as projectile fragmentation or target evaporation, probably contribute significantly to these parts of the spectra.

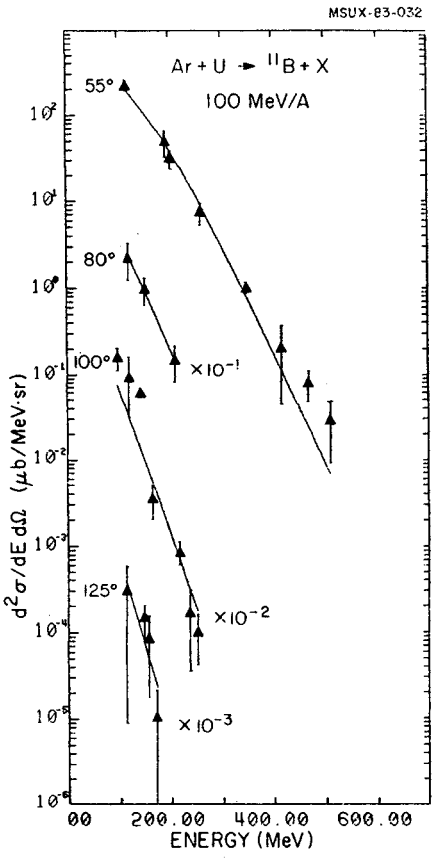

Fig. 2.

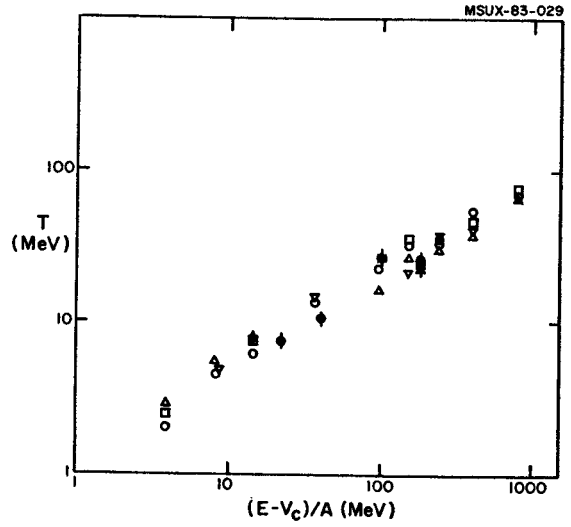

Fig. 3. Variation with incident energy of the temperature of the moving source, as obtained from the simple moving source parameterization. The solid points are for the systems discussed in the text, the other are taken from ref. 2. Symbols are the same as in Fig. 4.

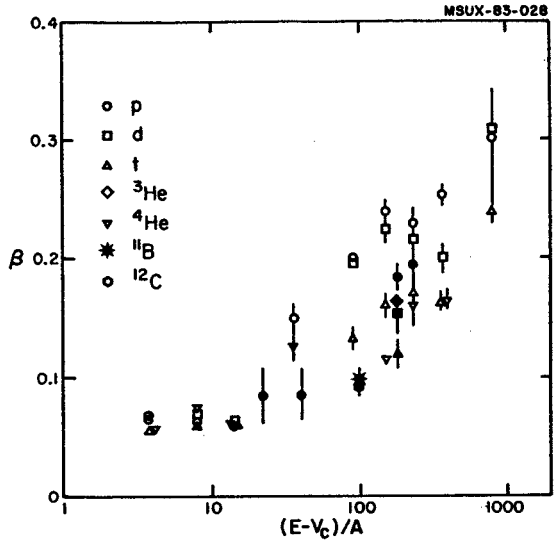

Fig. 4. Variation with incident energy of the moving source velocities, obtained from the moving source parameterization. The solid points are for the systems described in the text. The others are taken from ref. 2.

Our analysis helps to reinforce the validity of a localized, thermal source. The existence of this source is important to the development of thermal and hydrodynamical description of heavy-ion collisions. The emission of heavy composite fragments may be particularly interesting for the study of liquid gas phase transitions in nuclear systems.[7]

1. T.C. Awes, G. Poggi, G.K. Gelbke, B.B. Back, B.G. Glagola, H. Breuer, V.E. Viola, Phys. Rev. C24 (1981), 89.
2. G.D. Westfall, B.V. Jacak, N. Anantaraman, M.W. Curtin, G.M. Crawley, C.K. Gelbke, B. Hasselquist, W.G. Lynch, D.K. Scott, B.M. Tsang, M.J. Murphy, T.J.M. Symons, R. Legrain, T.J. Majors - to be published.
3. N. Stelte and R. Weinert, Preprint, 1982.
4. K.R. Cordell, S.T. Thornton, L.C. Dennis, R.R. Doering, R.L. Parks and T.C. Schweitzer, Nucl. Phys. A362 (1981) 431.
5. K.A. Frankel and J.D. Stevenson, Phys. Rev. C 23 (1981), 1511.
6. R. Santo, private communication, 1982.
7. M. Curtin, H. Toki and D.K. Scott, MSU Preprint and this Report, page

Angular Distribution of Pions from Subthreshold Production with Heavy Ions

W. Benenson, G.M. Crawley, E. Kashy, J.A. Nolen, D. Murphy[x], J.A. Bistirlich[x], H.R. Bowman[x], K.M. Crowe[x], J.O. Rasmussen[x], J.P. Sullivan[x], W.A. Zajac[x], J.P. Miller[+], O. Hashimoto[xx], M. Koike[xx], and J. Peter[++].

As part of a study of pion production below the nucleon-nucleon threshold with heavy ions, we have analyzed data from an angular distribution at E/A=138 MeV for ^{20}Ne+NaF. The data were taken at the LBL Bevalac by a MSU-LBL-Orsay-Tokyo collaboration. The results can be summarized as follows: 1) There is a very large π^-/π^+ ratio at 0^o indicating that cold charged parojectile fragments still exist after the collision even at this low energy. 2) The angular distribution is isotropic in the center of mass frame for a fixed pion momentum in that frame, which may indicate a predominance of thermal production rather than first collision nucleon-nucleon production. 3) The magnitude of the cross section is in good agreement with previous work[1] and is smaller than the full firestreak calculation[2] with all composite particles and resonances as can be seen in the figure. The amount and type of composite particles included affects the pion cross section very strongly because of the very strong temperature dependence. This can be seen on the figure by comparing firestreak calculations with and without α's, t's and ^{3}He's. The curve labelled thermal comes from the model of Kapusta[3] and the curve labelled Hecking[4] is a first collision + thermal calculation.

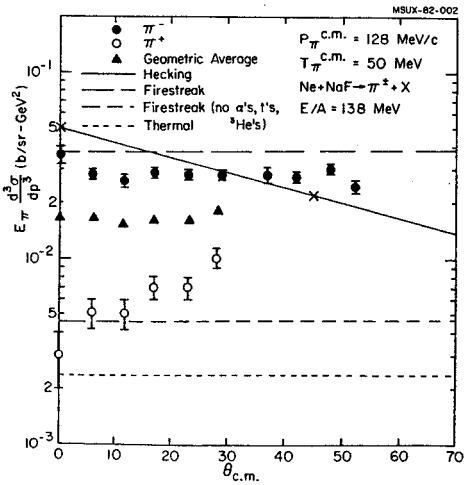

Fig. 1. Invariant cross section versus angle in the N-N center of mass for π^+ and π^- produced in Ne+NaF collisions at E/A = 138 MeV.

x LBL Berkeley
\+ Boston University
xx INS Tokyo
++ IPN Orsay

1. W. Benenson, G. Bertsch, G.M. Crawley, E. Kashy, J.A. Nolen, Jr., H. Bowman, J.G. Ingersoll, J.O. Rasmussen, J. Sullivan, M. Koike, M. Sasso, J. Peter, T.E. Ward, Phys. Rev. Lett. 43, 683 (1979), 44, 54 (1980).
2. G.D. Westfall, J. Gosset, P.J. Johansen, A.M. Poskanzer, W.G. Meyer, H.H. Gutbrod, A. Sandoval and R. Stock, Phys. Rev. Lett. 37, 1202 (1976).
3. J.I. Kapusta, Phys. Rev. C16, 1493 (1977).
4. P. Hecking, LBL-12671 and private communication.

Anomalons as Pineuts

Wm. C. McHarris* and J.O. Rasmussen+

"Anomalons" is the name given to those projectile fragments that have anomalously short mean free paths immediately following their formation in relativistic heavy-ion collisions[1]. First seen in cosmic-ray experiments, they have been corroborated by groups working with relativistic heavy-ion beams, in particular at the LBL Bevalac. Anomalons have produced considerable interest, for they are difficult to explain. Indeed, Ref. 1 concludes: "We are thus left in a predicament. Conventional nuclear physics as well as systematics fail to explain the observations..."

To be considered viable, any explanation must be able to account for the following six points:

1) The energy range of production, i.e., $E \approx 1\text{-}2$ AGeV.

2) The anomalously short mfp's themselves. (If this were purely a size effect, an increase of 50% in reaction cross-section would imply a decrease of $\approx 70\%$ in the nuclear density.)

3) The average length of the "decay" paths, implying a mean lifetime of $\gtrsim 10^{-10}$ sec.

4) No charged particles emitted in the "decay" of anomalons.

5) The enhancement of the anomalon effect for fragments of low charge; however, with a drop-off at or exclusion of charges 2 and 1.

6) The existence of a memory effect; i.e., enhancement of the anomalon effect for tertiary and later generations produced by secondary fragments that were anomalons themselves.

Actually, there have been a number of suggested explanations, which range from postulating quasi-molecular nuclei and "bubble" nuclei to postulating the existence of a new topological quantum number. Mostly, they focus on rearrangements of quark states and on quantum chromodynamics. The difficulty is that none of them adequately explains the experimental observations.

We have proposed a possible explanation[2] for anomalons, which falls within the framework of "conventional" nuclear physics and requires no exotic or esoteric additions. Further, at least qualitatively, it explains the important six points above.

Anomalons could well result from a nuclear halo of "pineuts", hadronically bound states of a π^- and a few neutrons surrounding a nucleus. Although the s-wave π^--n interaction is repulsive, the p-wave is attractive. Thus, the possibility exists that neutron-rich nuclei (or nuclei with locally neutron-rich domains, such as the neck in a fissioning system) might have a sufficiently attractive velocity-dependent potential to allow π^--xn hadronically bound "polyneutron" systems. This possibility was first considered by Ericson and Myhrer, who noted that a finite piece of nuclear matter might bind a π^- at lower than nuclear density and without absorption (or with diminished absorption). (Normally, even if such states were to exist, one would expect them to be strongly damped because of the strong absorption.) Based on a particular parameterization of the optical potential, they concluded that, although strongly-bound π^--nuclear states ought to exist in some neutron-rich medium-weight nuclei, such states would be the exception rather than the rule. Shortly thereafter, Friedman, Gal, and Mandelzweig, using a different parameterization taking into account new, precise data on 2p levels in pionic atoms, concluded that strongly-bound π^--nuclear systems should be the rule rather than the exception. The widths they obtained for such states, however, were prohibitively large for their observability except possibly in heavy nuclei. There have since been suggestions for experiments in which to look for π^--xn ("pineut") systems -- these focused on searching for negatively-charged free π^--polyneutrons, which cannot decay by the strong interaction. (If the binding energy were to exceed the π-μ mass difference of 33.9 MeV, the weak-decay channel closes, as well.)

Relativistic heavy-ion collisions provide the best opportunity for forming such states, for it has been found that not only are π^-'s produced in copious quantities in these collisions, but also they are Coulomb-focused near the same velocity as the projectile and target fragments (as opposed to π^+'s, which are defocused). Thus, the target nuclei are bathed in a localized, intense flux of π^-'s. Further, the excited nuclear fragments may have neutrons in barely-bound orbitals with wave-functions tailing out well beyond the normal nuclear radius. (The Coulomb potential will relatively suppress the analogous tailing out of the proton wave-functions.) Whether or not free π^--xn clusters are bound, the conditions are optimal for forming a nuclear stratospheric halo enriched in pineut clusters.

This explanation of anomalons meets the six requisite conditions as follows:

1) The production energy range is satisfied. The π^-'s are produced abundantly above the $\Delta(1232)$ threshold ($\approx$0.7 AGeV lab). Note that the anomalon observations are below the region of abundant associated production of kaons and lambdas and below the threshold for producing anti-protons, so alternative explanations in terms of quark rearrangements encounter more

serious difficulties.

2) We know that ordinary pionic atoms' lifetimes are not long enough to allow such atoms to qualify as anomalons, unless they were to have the π^- in rather high Rydberg orbitals. For example, Fig. 8 of Backenstoss (cf.Ref. 2) shows widths of ≈1 keV and 0.7 eV for the 2p and 3d levels, respectively, of Z=20. Possibly the 4f levels could approach having anomalon lifetimes, but there seems no likelihood of injecting π^-'s into high Rydberg orbitals in the numbers needed to explain the ≈6% anomalon component. We thus turn for a model to a π^--dineutron (or possibly π^--polyneutron) cluster orbiting the nucleus at a distance such that the overlap of the π^- with any proton wave-function is small. This larger object would clearly exhibit an enlarged cross-section on emulsion nuclei, but it would cause reactions of the ordinary sort, as required by observations on anomalons. Examination of the shell-model level diagrams of Meldner shows usually at least one oscillator shell of bound but unoccupied neutron levels above the normally occupied levels. For excited nuclei or nuclei nearer the neutron drip line we may find slightly bound, large neutron orbitals exponential, the r.m.s. radius = $3.23\ B_n^{-1/2}$ fm, with B_n in MeV.

3) The mean life of a free π^- is 26 nsec, and in a "free" pineut system (without protons and absorption), this would be increased as the binding energy is increased. (The phase space for weak decay would decrease until the π-μ mass difference was reached, whereupon such a "free" system would become stable with respect to this decay mode.) In the proposed pineut/anomalon systems, however, there <u>are</u> protons, and the limiting factor will be keeping the π^--p wave-function overlap as small as possible. Lifetimes of $\geq 10^{-10}$ sec might be attained for non-s-wave pineut orbitals outside the parent nucleus. That this is true is demonstrated by the behavior of π^-'s on the lightest elements. The intrinsic odd parity of the pion necessitates that it annihilate from at least a p-state, which introduces geometrical complications that retard the decay. [See also under point 4).]

4) The predominant decay mode of the orbiting pineut might well be a neutral decay, with the π^- mass being given to a pair of neutrons, as occurs with pionic ^{2}H. This decay mode occurs by interaction of the π^- with the virtual π^+ of a proton in a correlated p-n pair, necessary for the conservation of momentum. (This capture mode is most often accompanied by some photon emission.) There is also the possibility of a 2γ branching mode if the π^- charge exchanges on a proton to form a π^o, which subsequently decays. This decay mode occurs of necessity with pionic ^{1}H, but it has also been seen from pionic ^{3}He, where the p-n correlation introduces geometrical complications. These decay modes are discussed in greater detail elsewhere.

5) The peaking of the effect for low-charge fragments follows straightforwardly, for the pineut halo would have the greatest effect as part of a small fragment. The effect would lessen as the size of the fragment increased, so that the mfp's of anomalons would tend to become rather independent of charge, as has been, in fact, observed. On the other hand, the diminished effect (if any effect does exist) for charges smaller than 3 also follows, for here the requisite neutron excess (or tailing of the neutron wave-functions) is not available.

6) The existence of memory enhancement is also a straightforward consequence of our model. A prime requisite for the anomalon effect is this neutron excess (or tailing). This would be expected to persist more or less from generation to generation.

Several predictions and tests of our explanation come to mind immediately. First, the anomalon effect should be enhanced whenever there is an excess of neutrons. Thus, the effects from neutron-rich beams such as ^{48}Ca should be investigated, and comparisons between, say, ^{40}Ca and ^{48}Ca beams should be made. Also, very heavy beams such as ^{238}U should be tested, for these provide very neutron-rich domains, especially in their necks while fissioning. Second, photons from the radiative capture or charge exchange mode should be looked for. A shadowed, drift experiment downstream from the target could possibly enable these to be seen above the photon background from other effects--for example, those originating from the decay of free π^o's. (See below for the recent results from such an experiment.) Third and finally, the falling off of the anomalon effect with very small charge should be examined very carefully, inasmuch as our model predicts that the effect should be quite small, if not vanishingly small, for ^{4}He and especially for ^{3}He.

Since first issuing our proposed explanation, we have been performing some relatively simple and qualitative calculations, and the preliminary results are encouraging. Using the most recent pion-nucleus optical potential[3], we are not only able to obtain sufficient binding, but also we find that we get a singular point in the wave function near the "normal" nuclear radius, which effectively shields the π^-'s from the proton density farther in. In addition, there is the likely possibility that certain spin-isospin [(3,0) and (0,3)] Δ-Δ combinations yield deeply bound states[4]. We plan to continue our investigations and calculations along this line.

The evidence for our explanation must necessarily remain qualitative and of a negative sort

for the present. For example, a recent experiment to search for delayed α-rays following the production of anomalons produced a negative result[5], and its authors conclude that most of the explanations, other than ours, are inconsistent with their results. This is by no means proof that we are correct, but it is most encouraging.

---

* Work performed while on sabbatical leave at Lawrence Berkeley Laboratory, 1981-82.
+ Nuclear Science Division, Lawrence Berkeley Laboratory, and Department of Chemistry, University of California, Berkeley.

1. E.M. Friedlander, R.W. Gimpel, H.H. Heckman, Y.J. Karant, B. Judek, and E. Ganssauge, Phys. Rev. Lett. 45, 1084 (1980); E.M. Friedlander, H.H. Hickman, Y.J. Karant, and B. Judek, LBL Report No. LBL-10573 (1982).
2. Wm. C. McHarris and J.O. Rasmussen, LBL Report No. LBL-14075 (submitted to Phys. Lett. 1982). This report contains extensive references to the literature on anomalons and explanations for them; thus, we do not reproduce these references here.
3. J.A. Carr, H. McManus, and K. Stricker-Bauer, Phys. Rev. C 25, 952 (1982).
4. T. Kamae and T. Fujita, Phys. Rev. Lett. 38, 471 (1977).
5. T.M. Liss, S.P. Ahlen, P.B. Price, and G. Tarle, Lawrence Berkeley Laboratory, preprint (1982).

Comment on Evidence for anomalous nuclei among relativistic projectile fragments from heavy-ion collisions at 2 GeV/nucleon

D. J. Morrissey

Friedlander et al. have shown evidence for diminution of the mean free path (mfp) of projectile fragments (PF) emerging from reactions of high energy heavy-ions in emulsion.[1] The mean free paths of PF's start out approximately 15 percent shorter than previous measurements of the mean free paths of heavy beams of similar nuclei. This "shortness" subsequently appears to decay away with distance (or time) from the initial interaction. The authors comment that they are not aware of explanations within the framework of conventional nuclear physics for their results.[1] A simple explanation consistent with the logarithmic growth of the mfp after the interaction is that the PF's are created with some intrinsic angular momenta which causes the nuclei to stretch to an equalibrium shape. The angular momentum is then removed by the familar gamma-ray cascade on a time scale characterized by the lifetimes of the excited states of the PF's. Upon reaching their ground states the PF's are truely similar to "normal beam nuclei" and exhibit the same mfp. The lifetimes of excited states at a few ħ in nuclei with masses comparable to RF's masses are on the order of tens of picoseconds. This is exactly equal to the lifetime of the anomalous behavior estimated by Friedlander et al.[1] Unfortunately a direct check of the present suggestion is not possible at present because the spins produced in the PF's by relativistic heavy-ion reactions are not known. A check on the plausibility of the suggestion can be made by estimating the magnitude of the spin necessary to account for the observed effect.

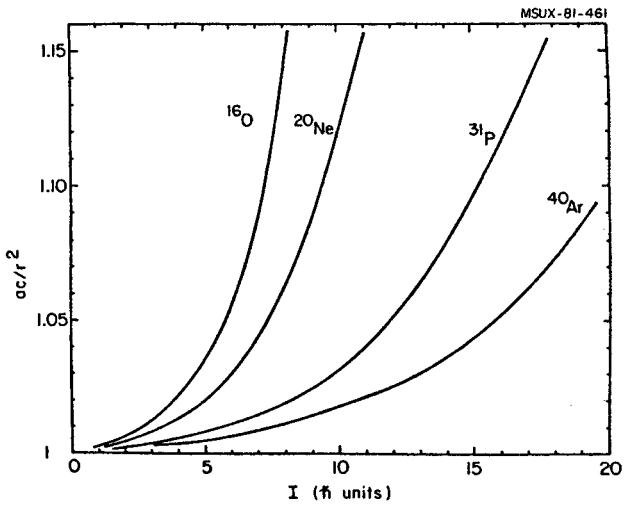

Fig. 1. The increase in area expected for spin I relative to that of a spherical nucleus is shown for several light nuclei.

The mfp is inversely proportional to the cross section, thus the ratio of the anomalous reaction cross section to that of normal beam nuclei is $\sigma_A/\sigma_B = \Lambda_B/\Lambda_A \sim 1.15$. In other words an increase in the area of PF's by only 15 percent is required by the data. All models of projectile fragmentation require that the interaction be peripheral. The angular momentum generated by the highly localized forces will be oriented perpendicular to the direction of linear motion. Such rotating nuclei will stretch, in the liquid drop model,[2,3] to find the equilibrium shape dictated by the rotational, Coulomb and surface energies. The stretched nuclei will have a larger cross sectional area which will decrease as the intrinsic angular momentum is removed by gamma-rays. The ratio of the area of a spheriod with semi-major axes a = b≠c to that of a sphere with the same volume[2] is shown as a function of spin in Fig. 1. Rigid body moments of inertia have been assumed. Such calculations should be taken with a grain of salt when applied to nuclei as light as oxygen, but are instructive none the less. From Fig. 1 the order of magnitude estimate of the spin necessary to stretch an average of PF enough to create the shorter mfp is only ~ 10ħ.

The question finally becomes is the spin necessary to stretch the PF's by ≈ 15 percent, namely 10h, within reach of the collision process? A simple estimate of the amount of angular momentum imparted to a fragment[4], $L \approx R \times p \approx 5\hbar$ indicates that the suggestion is reasonable and consistent with current knowledge of relativistic heavy-ion reactions.

1. E.M. Friedlander et al. Phys. Rev. Lett. 45, 1084 (1980).
2. B. Nilsson, Nucl. Phys. A129, 445 (1968).
3. W.D. Meyers and W.J. Swiatecki, Annl. Phys. (NY) 84, 186 (1974).
4. T. Shibata et al. Nucl. Phys. A308, 513 (1978).